

1 **Size distribution and optical properties of mineral dust** 2 **aerosols transported in the western Mediterranean**

3
4 C. Denjean^{1,2}, F. Cassola³, A. Mazzino³, S. Triquet¹, S. Chevaillier¹, N. Grand¹, T. Bourrienne⁴,
5 G. Momboisse⁴, K. Sellegri⁵, A. Schwarzenbock⁵, E. Freney⁵, M. Mallet⁶ and P. Formenti¹

6
7 [1] Laboratoire Interuniversitaire des Systèmes Atmosphériques (LISA), UMR-CNRS 7583,
8 Université Paris-Est-Créteil (UPEC) et Université Paris Diderot (UPD), Institut Pierre Simon
9 Laplace (IPSL), Créteil, France

10 [2] Leibniz Institute for Tropospheric Research (TROPOS), Permoserstraße 15, 04318, Leipzig,
11 Germany

12 [3] Department of Physics and INFN, Genoa, Italy

13 [4] Centre National de Recherches Météorologiques (CNRM), Météo-France, Toulouse, France

14 [5] Laboratoire de Météorologie Physique (LaMP), CNRS/Université Blaise Pascal, Clermont-
15 Ferrand, France

16 [6] Laboratoire d'Aérodologie (LA), Université de Toulouse, CNRS, Toulouse, France

17
18 Correspondance to :

19 Cyrielle Denjean (cyrielle.denjean@meteo.fr), Paola Formenti (paola.formenti@lisa.u-pec.fr)

1 **Abstract**

2 This study presents *in situ* aircraft measurements of Saharan mineral dust transported over the
3 western Mediterranean basin in June-July 2013 during the ChArMEx/ADRIMED (the
4 Chemistry-Aerosol Mediterranean Experiment / Aerosol Direct Radiative Impact on the
5 regional climate in the MEDiterranean region) airborne campaign. Dust events differing in
6 terms of source region (Algeria, Tunisia and Morocco), time of transport (1-5 days) and height
7 of transport were sampled. Mineral dust were transported above the marine boundary layer,
8 which conversely was dominated by pollution and marine aerosols. The dust vertical structure
9 was extremely variable and characterized by either a single layer or a more complex and
10 stratified structure with layers originating from different source regions. Mixing of mineral dust
11 with pollution particles was observed depending on the height of transport of the dust layers.
12 Dust layers carried higher concentration of pollution particles below 3 km above sea level (asl.)
13 than above 3 km asl., resulting in scattering Angstrom exponent up to 2.2 below 3 km asl..
14 However, the optical properties of the dust plumes remained practically unchanged with respect
15 to values previously measured over source regions, regardless of the altitude. Moderate
16 absorption of light by the dust plumes was observed with values of aerosol single scattering
17 albedo at 530 nm ranging from 0.90 to 1.00 ± 0.04 . Concurrent calculations from the aerosol
18 chemical composition revealed a negligible contribution of pollution particles to the absorption
19 properties of the dust plumes that was due to a low contribution of refractory black carbon in
20 regards to the fraction of dust and sulfate particles. This suggests that, even in the presence of
21 moderate pollution, likely a persistent feature in the Mediterranean, the optical properties of the
22 dust plumes could be assumed similar to those of native dust in radiative transfer simulations,
23 modeling studies and satellite retrievals over the Mediterranean. Measurements also showed
24 that the coarse mode of mineral dust was conserved even after 5 days of transport in the
25 Mediterranean, which contrasts with the gravitational depletion of large particles observed
26 during the transport of dust plumes over the Atlantic. Simulations with the WRF mesoscale
27 meteorological model highlighted a strong vertical turbulence within the dust layers that could
28 prevent deposition of large particles during their atmospheric transport. This has important
29 implications for the dust radiative effects due to surface dimming, atmospheric heating and
30 cloud formation. The results presented here add to the observational dataset necessary for
31 evaluating the role of mineral dust on the regional climate and rainfall patterns in the western
32 Mediterranean basin and understanding their atmospheric transport at global scale.

33
34

1 **1. Introduction**

2 Mineral dust aerosols constitute a major fraction of airborne particulate matter (Huneeus et al.,
3 2012) and their contribution to the Earth's climate system is of considerable significance. In
4 particular, dust aerosols exert a significant effect on global radiative budget by scattering and
5 absorbing longwave and shortwave radiation (IPCC, 2013), thereby impacting the vertical
6 profile of temperature and atmospheric stability (Jing et al., 2008) and the precipitation rate
7 (Rosenfeld et al., 2001; Andreae and Rosenfeld, 2008; Choobari et al., 2014).

8 The Sahara desert hosts the maximum dust emission and atmospheric dust loading in the world
9 (Choobari et al., 2014). Strong winds and convection produced by intense surface heating can
10 uplift mineral dust particles into the free troposphere, where they are advected over large
11 distances at the continental and intercontinental scales (d'Almeida, 1986; Goudie and
12 Middleton, 2001; Engelstaedter et al., 2006). Along the year, the transport pathway of Saharan
13 dust is mainly controlled by low-pressure systems over the Atlantic or North Africa, high
14 pressure over the Mediterranean region, or high pressure at upper level over Africa (Moulin et
15 al., 1998; Querol et al., 2009; Salvador et al., 2014). A significant fraction of dust loaded from
16 Africa sources are transported westward across the Atlantic Ocean as far as the Caribbean
17 (Maring et al., 2003; Doherty et al., 2008), the United States (Perry et al., 1997; Prospero et al.,
18 2002) and South America (Swap et al., 1992; Formenti et al., 2001; Ansmann et al., 2009).
19 Large Saharan dust storms are also carried across the Mediterranean Sea to Europe (Moulin et
20 al., 1998; Koren et al., 2003; Collaud Coen et al., 2004; Van Dingenen et al., 2005; Papayannis
21 et al., 2008). During such outbreaks, mineral dust emerges as the largest PM₁₀ source at rural
22 and urban sites in the Mediterranean basin (Pey et al., 2013; Salvador et al., 2014).

23 Considerable uncertainties in quantifying the climatic effect of mineral dust arise from a lack
24 of knowledge of their properties and spatial and vertical distributions over many regions of the
25 world. In particular, to estimate the magnitude of the dust radiative effect, an accurate
26 description of both particle size distribution and optical properties and their link with the
27 chemical composition is necessary (Sokolik and Toon, 1996; Tegen et al., 1996). The size
28 distribution is a fundamental parameter to estimate the aerosol radiative effect and atmospheric
29 lifetime, but its representation remains challenging due to the large size spectrum of mineral
30 dust, from hundreds of nanometers to tenths of micrometers (Formenti et al., 2011a). In
31 particular, an accurate description of the coarse mode particles is vital since the presence of
32 large particles enhance the capacity of mineral dust in absorbing radiation at short and long
33 wavelengths (McConnell et al., 2008; Otto et al., 2009; Sicard et al., 2014), modify the
34 atmospheric heating rate (Ryder et al., 2013a) and affect cloud formation (Koehler et al., 2009).

1 Once in the atmosphere, mineral dust can undergo various aging processes, such as
2 heterogeneous reactions with gas-phase compounds (Sullivan and Weber, 2006; Ma et al.,
3 2012), condensation of low-volatile species (Bauer et al., 2004; Clarke et al., 2004; Sullivan
4 and Prather, 2007), cloud processing (Levin et al., 1996; Trochkin et al., 2003) and coagulation
5 (Fan et al., 1996; Zhou et al., 1996; Levin et al., 2005). Because of these processes, the physico-
6 chemical properties (composition, mixing state, shape, and size distribution) of dust aerosols
7 might evolve during transport, leading in turn to the evolution of the optical properties
8 (Formenti et al., 2011a). A recent study of Kanitz et al. (2014) has shown significant differences
9 in the optical properties of two Saharan dust plumes over the Atlantic Ocean, resulting from
10 different aging processes affecting the dust. Henceforth, the radiative effect of mineral dust
11 should depend on the travel distance and pathway, residence time over their source regions and
12 air masses encountered (Garrett et al., 2003).

13 The Mediterranean basin provides ideal conditions to investigate the changes in Saharan dust
14 properties as numerous concurrent anthropogenic and natural sources of aerosols are active over
15 this region. Case studies of mixing of Saharan dust with industrial/urban, marine and biomass
16 burning particles have been documented in the past (Koçak et al., 2012; Mantas et al., 2014),
17 and could explain the large variability of the values of single scattering albedo ω (0.83-0.92 at
18 the wavelength of 440 nm) reported by various studies (Sicard et al., 2012; Mallet et al., 2013).
19 In past years, intensive field campaigns including *in situ* airborne measurements have mostly
20 focused on properties of mineral dust at emission (e.g., over the Saharan and the Sahelian source
21 regions) and over the Atlantic Ocean, and their comparison to trace the temporal evolution
22 during transport (Formenti et al., 2003, 2011b; Reid et al., 2003; McConnell et al., 2008;
23 Osborne et al., 2008; Heintzenberg, 2009; Weinzierl et al., 2009, 2011; Haywood et al., 2011;
24 Ryder et al., 2013a,b). On the contrary, observations in the Mediterranean region were mostly
25 limited to remote sensing from the ground (e.g. Moulin et al., 1997; Hamonou et al., 1999;
26 Meloni et al., 2006; Saha et al., 2008; Basart et al., 2009; Gómez-Amo et al., 2011; Perrone and
27 Bergamo, 2011; Mallet et al., 2013; Pey et al., 2013; Marconi et al., 2014) or spaceborne (de
28 Meij and Lelieveld, 2011; Gkikas et al., 2012).

29 To fill this gap, the Aerosol Direct Radiative Impact on the regional climate in the
30 MEDiterranean region (ADRIMED) field campaign, part of the international cooperative
31 research program ChArMEx (the Chemistry-Aerosol Mediterranean Experiment;
32 <http://charmex.lsce.ipsl.fr>) took place with the main objectives of characterizing Saharan dust
33 plumes by coordinated aircraft and ground-based measurements (Mallet et al., 2015). In this
34 paper, we present *in situ* aircraft measurements obtained in June-July 2013 over the

1 Mediterranean basin. The objective is to determine possible changes of dust properties during
2 long-range transport over the western Mediterranean basin and explore the potential reasons for
3 changes.

4 Section 2 describes the aircraft strategy, the instrumentation and the method used to determine
5 the aerosol size distribution, chemical composition and the associated optical properties.

6 Section 3 presents the campaign meteorology, the dust vertical profiles and the results of the
7 aerosol properties within the dust plumes. Section 4 explores the potential factors affecting the
8 variability of the aerosol properties due to altitude and dust age. Section 5 concludes this article.

9

10 **2. Measurement and methodology**

11 **2.1. Aircraft strategy**

12 The ATR-42 aircraft of SAFIRE (French aircraft service for environmental research,
13 <http://www.safire.fr>) based at Cagliari (39°15'N, 9°03'E, Italy) conducted 16 flights in the
14 period 14 June - 04 July 2013. In this paper, we present results from the 9 flights dedicated to
15 the observation of mineral dust plumes that occurred between 16 June and 03 July 2013. These
16 flights were carefully selected to provide measurements of air masses from dust active sources
17 based on the analysis of satellite images and backward trajectories, as described in section 2.4.
18 The ATR-42 aircraft performed research flights in the area between 35° - 43° N and -4°- 13°
19 E, covering the western Mediterranean region to probe the Saharan dust properties in a range
20 of varying transport pathways and source regions. The flight tracks are shown in Figure 1 and
21 a summary of flight information is provided in Table 1.

22 The airborne missions were planned using four different dust plume forecast models (MACC
23 ALADIN-Dust, SKIRON and BSC-DREAM8b v2.0) and satellite images from the SEVIRI
24 radiometer on the Meteosat Second Generation (MSG) satellite, all available in real time from
25 the ChArMex Operating Center (<http://choc.sedoo.fr/>) during the campaign. The general
26 weather forecast was made daily by the French school of Meteorology (ENM), at Météo-France
27 in Toulouse.

28 The general flight strategy consisted of two main parts: first, profiles from 300 m up to 6 km
29 above sea level (asl) were conducted by performing a spiral trajectory 10-20 km wide to sound
30 the vertical structure of the atmosphere and identify interesting dust layers. Afterwards, the
31 identified dust layers were probed by straight levelled runs (SLR), where the aircraft flew at
32 fixed altitudes, to provide information on dust spatial variability and properties. Horizontal
33 flight legs in the dust layers lasted 20-40 min to allow aerosol collection on filters. At the typical
34 aircraft cruise speed of 100 m s⁻¹, samples had spatial resolution ranging from 121 to 242 km.

1
2
3
4
5
6
7
8
9
10
11
12
13
14
15
16
17
18
19
20
21
22
23
24
25
26
27
28
29
30
31
32
33
34

2.2. Instrumentation

The ATR-42 basic instrumentation provides meteorological parameters including temperature, dew point temperature, pressure, turbulence, relative humidity, wind speed, direction, CO and O₃ concentrations (Saïd et al., 2010). Only instruments relevant to microphysical properties, chemical composition and optical properties of aerosols are detailed in Table 2.

2.2.1. Aerosol concentration and size distribution

The total number concentration of particles larger than 5 nm in diameter was measured using a butanol-based condensation nucleus counter (CPC, TSI model 3075) corrected for coincidences.

The particle number size distribution was measured over the largest possible size spectrum by combining optical and electrical mobility techniques.

The number size distribution in the submicron range was measured with an in-cabin Scanning Mobility Particle Sizer (SMPS) and a wing-mounted Ultra High Sensitivity Aerosol Spectrometer (UHSAS, Droplet Measurement Technologies). The SMPS consisted of a Differential Mobility Analyzer (DMA, Villani et al., 2007) interfaced to a Condensation Particle Counter (CPC, TSI model 3010). A closed-loop recirculation was used for the sheath flow of the DMA. The SMPS system provided the number size distribution of the electrical mobility diameter from the 30 - 400 nm in 135 nominal size classes (i.e. size classes provided by the instrument not corrected for the dynamic shape factor) over time scans lasting 120 seconds. Therefore, only data acquired during SLR are considered. Data were processed by taking into account the particle electrical charging probabilities, the CPC counting efficiencies, the DMA transfer functions and the diffusion losses in the SMPS and CPC systems. The UHSAS is an optical-scattering laser-based aerosol spectrometer, providing the number size distribution of the optical equivalent diameter from 0.04 to 1 µm in 99 nominal size classes at a time resolution of 1 second. The spectrometer integrates light scattering between 22 to 158° at 1054 nm. Due to reduced counting efficiency at size larger than 0.9 µm, only data at lower sizes are considered in this paper. The uncertainties on the particle diameter were estimated to be 5% and 10% for the SMPS and UHSAS, respectively (Wiedensohler et al., 2012; Cai et al., 2008).

The number size distribution in the supermicron range was measured by the combination of two different optical particle counters (OPC). A wing-mounted Forward Scattering Spectrometer Probe (FSSP, Particle Measuring System, Model 300) measured the optical size

1 distribution in the nominal size range of 0.28 to 20 μm (Baumgardner et al., 1992). Data were
2 recorded in 30 size classes at 1 second interval. The FSSP-300 is based on the measurement of
3 the light scattered between 3 and 12° at 632.8 nm. The FSSP has an uncertainty in diameter of
4 about 30 % according to Baumgardner et al. (1992). A GRIMM OPC (model sky-OPC 1.129)
5 operated inside the cabin at a 6-second time resolution and measuring the optical size
6 distributions between 0.3 and 32 μm on 32 size classes in nominal diameter. However, only
7 data at nominal size below 12 μm were considered here due to the passing efficiency of the
8 aerosols inlets connected to the GRIMM (see section 2.3.2. for further information). The
9 instrument integrates light scattering between 30 and 150° at 655 nm. According to the
10 calibration of the GRIMM with standard, we assumed an uncertainty in diameter of 10%.

11

12 **2.2.2. Aerosol chemical composition**

13 Bulk aerosol samples were collected on-board by filtration through two stainless-steel filter
14 units mounted in parallel. Sampling was performed only during constant altitude sequences
15 lasting more than 25 minutes in order to guarantee sufficient mass loading of the filter samples.
16 After exposure, samples were stored and transported at -20°C to avoid later modification. Once
17 in the laboratory, samples collected on 42-mm diameter polycarbonate membranes (nominal
18 pore size 0.4 μm Nuclepore, Whatman) were cut in halves that were analyzed to yield the
19 elemental and ionic composition. Concentrations of elements from Na to Pb were measured by
20 wavelength-dispersive X-ray fluorescence (WD-XRF) using a PW-2404 spectrometer
21 (Panalytical). Details of the analytical protocols are provided by Formenti et al. (2008). The
22 concentration of water-soluble ions were determined by Ion chromatography (IC) with a
23 Metrohm IC 850 device equipped with an injection loop of 100 μl . For anionic species, IC has
24 been equipped with Metrosep A supp 16 (250/4.0mm) column associated with a metrosepA
25 supp 16 guard pre-column heated at 65°C. For simultaneous separation of inorganic and short-
26 chain organic anions, elution has been realized with eluant composed at 20% by ultrapure water
27 and at 80% by a solution 7.5 mM Na_2CO_3 and 0.75mM NaOH. The elution flow rate was 0.8
28 mL min^{-1} . For cationic species, IC has been equipped with a Metrosep C4 (250/4.0mm) column
29 associated to a metrosep C4 guard column heated at 30°C. Elution has been realized with an
30 eluant composed with 0.7 mM of dipicolinic acid and 1.7 mM of nitric acid. The elution flow
31 rate was 1 mL min^{-1} .

32 The mass concentration of refractory black carbon particles (rBC) was measured using a single
33 particle soot photometer (SP2, DMT). The SP2 uses a continuous intra-cavity Nd:YAG laser at
34 the wavelength of 1064 nm to heat rBC-containing particles to their vaporization point. Single

1 particle rBC mass was derived from the peak intensity of the thermal radiation emitted by the
2 incandescent rBC detected by the SP2. This method allows the quantification with 100%
3 efficiency of rBC mass in single particles with mass equivalent diameters between 80-500 nm
4 (Moteki and Kondo, 2010). The total rBC mass loading was reported as the sum of all the
5 detected single particle rBC masses. Prior to the measurement field campaign, the SP2 was
6 calibrated using fullerene soot particles, which have been shown to give similar SP2 response
7 as ambient rBC (Moteki and Kondo, 2010; Baumgardner et al., 2012; Laborde et al., 2012).

9 **2.2.3. Aerosol scattering and extinction coefficients**

10 The particle scattering coefficient (σ_{scat}) was measured at three wavelengths (450, 550 and 700
11 nm) with an integrating nephelometer (TSI, model 3563), which integrates light scattered by
12 particles at scattering angle between the incident and scattered radiation between 7° and 170° .
13 The instrument operated at a volumetric flow rate of 30 L min^{-1} and the data were acquired at
14 1-s time resolution. The instrument was calibrated with free-particle air and high-purity CO_2
15 prior to and after the campaign. Uncertainty in σ_{scat} measured with the nephelometer is
16 estimated to be 5% (Muller et al., 2011a). Measured values were corrected for the angular
17 truncature error in the nephelometer measurements at angles smaller than 7° and greater than
18 170° as described in section 2.3.2.

19 The particle extinction coefficient (σ_{ext}) was measured with a Cavity Attenuated Phase Shift
20 particle light extinction monitor (CAPS-PMex, Aerodyne Research) operated at the wavelength
21 of 530 nm. The instrument relies on measuring the average time spent by the light within the
22 sample cell. The sampling volumetric flowrate was 0.85 L min^{-1} and data were processed with
23 a time resolution of 1 second. Uncertainty in σ_{ext} measured with the CAPS is estimated to be
24 3% (Massoli et al., 2010).

26 **2.3. Aerosol data analysis**

27 Figure 2 depicts the iterative procedure used to retrieve the aerosol size distribution and optical
28 parameters relevant to this paper. We focused our attention on aerosol parameters used in
29 climate models for calculating the direct and semi-direct aerosol radiative effects:

- 30 - The complex refractive index \tilde{n} defined as $n_r - in_i$, where n_r and n_i are the real and imaginary
31 part representing the particle scattering and absorption properties, respectively.
- 32 - The single scattering albedo ω_0 (unitless) representing the balance between the scattering and
33 the absorbing properties and defined as:

$$\omega_0(\lambda) = \frac{\sigma_{scat}(\lambda)}{\sigma_{ext}(\lambda)} \quad (1)$$

1 where σ_{scat} is the aerosol scattering coefficient (expressed in $Mm^{-1} = 10^{-6} m^{-1}$), σ_{ext} the aerosol
2 extinction coefficient (Mm^{-1}) and λ the wavelength (nm).

3 - The asymmetry parameter g (unitless) describing the angular distribution of the scattered
4 radiation and defined as:

$$g(\lambda) = \frac{1}{2} \int_0^\pi \cos(\Theta) \sin(\Theta) P(\Theta, \lambda) d\Theta \quad (2)$$

5 where $P(\Theta, \lambda)$ is the scattering phase function and Θ is the scattering angle.

6 - The mass extinction efficiency k_{ext} ($m^2 g^{-1}$) representing the total light extinction per unit mass
7 concentration of aerosol and calculated as:

$$k_{ext}(\lambda) = \frac{\sigma_{ext}(\lambda)}{C_m} \quad (3)$$

8 where C_m is the aerosol mass concentration ($\mu g m^{-3}$).

9 In this study, we have decided to neglect the non-sphericity of mineral dust since the sphere
10 model has been shown to produce negligible errors when computing radiative fluxes and flux
11 related quantities, i.e. aerosol optical depth (AOD), ω_0 and g (Mishchenko et al., 1995). Because
12 we only investigate angular-integrated properties and for sake of comparison with the large
13 majority of field data published so far, in this paper we only perform calculations in the
14 spherical approximation.

15

16 **2.3.1. Assessment of aerosol size distribution**

17 The particle size distribution was derived from the SMPS, UHSAS, GRIMM and FSSP-300.
18 For size distributions measured by SMPS, the electrical mobility D_m and the geometric particle
19 diameters D_g are related by the dynamic shape factor \mathcal{X} (DeCarlo et al., 2004):

$$D_g = \frac{D_m}{\mathcal{X}} \quad (4)$$

20 The dynamic shape factor \mathcal{X} depends on the shape of the particles (Hinds, 1999). In this study,
21 we have decided to neglect the non-sphericity of mineral dust to maintain retrieval conditions
22 similar to those of previous literature studies on dust in source region. Henceforth, \mathcal{X} was set
23 to unity.

24 Optical sizing instruments (i.e. UHSAS, GRIMM, FSSP-300) measure the amount of light
25 scattered by a single particle and convert this into a geometric particle size. This conversion
26 depends on the complex refractive index of the aerosol, as well as on the optical geometry and

1 the laser wavelength of the instrument. The correction procedure used the Mie scattering theory
 2 for homogeneous spheres with known complex refractive index (Bohren and Huffman, 1983).
 3 As discussed by Reid et al. (2003), the conversion of scattered light into particle size can lead
 4 to ambiguity in the sizing of the coarse mode diameters. If the light intensity response of the
 5 optical sizing instruments is non-unique it can lead to oversizing of larger particles. This
 6 happens mostly for forward scattering probes, such as the FSSP-300, as demonstrated in Figure
 7 S1 showing a flattening in the scattering cross section curves integrated over the FSSP-300
 8 scattering angle range (3-15°) between 2 and 10 μm diameter. For the GRIMM 1.129 scattering
 9 angles (30-150°), the scattering cross section is unique with size, except between 1.5-2 μm
 10 where an inflection point can be seen. During ADRIMED, systematic differences in the size
 11 distributions measured by the FSSP-300 and the GRIMM were observed around 2 μm. Given
 12 the response curves in Figure S1, data between 2-10 μm and 1.5-2 μm diameter from the FSSP-
 13 300 and the GRIMM, respectively, were not considered in this paper.

14 Figure 3 presents an example of size distributions measured in a dust plume by the different
 15 instruments. As will be discussed below, the value of $\tilde{n} = 1.53 - 0.004i$ at 530 nm was the most
 16 appropriate to reconstitute both scattering and extinction coefficient and therefore we present
 17 results using this value in Figure 3. Overall, the comparison between different instruments
 18 shows good consistency, giving credence to the measurements and the choice of refractive
 19 index and dynamic shape factor.

20 The resulting number and volume size distributions were parameterized by fitting four log-
 21 normal distributions, as:

$$\frac{dN}{d\log D_p} = \sum_{i=1}^4 \frac{N_{tot,i}}{\sqrt{2\pi} \cdot \log \sigma_i} \exp \left[-\frac{(\log D_p - \log D_{p,g,i})^2}{2(\log \sigma_i)^2} \right] \quad (5)$$

$$\frac{dV}{d\log D_p} = \sum_{i=1}^4 \frac{N_{tot,i} \cdot \frac{\pi}{6} \cdot D_p^3}{\sqrt{2\pi} \cdot \log \sigma_i} \exp \left[-\frac{(\log D_p - \log D_{p,g,i})^2}{2(\log \sigma_i)^2} \right] \quad (6)$$

22 each mode i being characterized by characterized by the integrated number concentration $N_{tot,i}$,
 23 the geometric median diameter $D_{p,g,i}$ and the geometric standard deviation σ_i (i.e. Figure 3).

24 To provide a synthetic representation of the particle number size distributions, the effective
 25 particle D_{eff} was calculated as :

$$D_{eff} = \frac{\int D_p^3 \frac{dN}{dD_p} dD_p}{\int D_p^2 \frac{dN}{dD_p} dD_p} \quad (7)$$

1 D_{eff} has been estimated separately on the fine and coarse fractions in the size ranges 0.053-1 μm
2 (referred as $D_{eff,f}$ thereafter) and 1-32 μm (referred as $D_{eff,c}$), respectively.

4 **2.3.2. Assessment of aerosol optical properties**

5 An iterative procedure was used to derive \tilde{n} , ω_0 , g and k_{ext} at 530 nm and correct σ_{scat} for the
6 angular truncature error (i.e. Figure 2). The parametrized size distributions were used as input
7 for the Mie scattering calculations (Bohren and Huffman, 1983), which were done by varying
8 stepwise the real part of the complex refractive index n_r from 1.33 to 1.60 and the imaginary
9 part of the complex refractive index n_i from 0.000 to 0.020. \tilde{n} was assumed to be constant with
10 particle size and have thus to be regarded as an effective value for the entire particle population.
11 σ_{scat} was adjusted to the CAPS operation wavelength of 530 nm by using the following equation:

$$\mathring{A}(\lambda_1, \lambda_2) = -\frac{\ln(\sigma_{scat}(\lambda_1)/\sigma_{scat}(\lambda_2))}{\ln(\lambda_1/\lambda_2)} \quad (8)$$

12 where \mathring{A} represents the spectral dependence of the scattering coefficient and λ_1 and λ_2 are the
13 wavelength interval. The scattering Angstrom exponent \mathring{A} is often used as a qualitative indicator
14 of aerosol particle size or fine mode fraction (Seinfeld and Pandis, 1998). Typically, it is lower
15 than ~ 0.5 for aerosols dominated by coarse particles, such as mineral dust or sea salt, but it is
16 higher than 1 for fine particles, such as pollution particles or biomass burning. The calculated
17 values of $\sigma_{scat}(530\text{nm})$ and $\sigma_{ext}(530\text{nm})$ were compared to that measured by the nephelometer
18 and the CAPS, and values having the closest agreement within the measurement error bars were
19 chosen as the best estimate.

20 The in-aircraft aerosol instruments sampled through isokinetic and isoaxial aerosol inlets. The
21 nephelometer and GRIMM were set up behind the AVIRAD inlet, while the CAPS, SMPS and
22 SP2 were set up behind the Community Aerosol Inlet (CAI). Particle loss can occur both as a
23 result of the inlet aspiration efficiency and the transport losses in the pipework between the inlet
24 and the instruments. The cut-off diameter, at which the passing efficiency of the inlet equals
25 50%, was determined by a set of wind-tunnel experiments (unpublished data). The passing
26 efficiency was determined as the ratio of the particle number concentration measured by
27 GRIMM optical counters behind the sampling lines of the AVIRAD and CAI inlets to the
28 particle number concentration measured in the main flow of the wing tunnel where the air speed
29 was 93 m s^{-1} as the cruise speed of the ATR-42. Monodisperse polystyrene latex spheres of 0.6,
30 1.2, 4.6, 7.9 and 11 μm diameter (Duke Scientifics, Thermo Sci.) and polystyrene
31 divinylbenzene spheres of diameter varying between 1 and 35 μm in diameter (also purchased
32 from Duke Scientifics) were first diluted and then put in a reservoir connected to a peristaltic

1 pump. The pump tubing was connected to a pneumatic spinning disk (SPIDI) in order to spray
2 a large amount of droplets from the solution, some droplets having a particle incorporated. An
3 air mover was mounted beneath the SPIDI and thus the droplets were rapidly evaporated. The
4 particle size-dependent passing efficiency of the AVIRAD and CAI sampling inlets shown in
5 Figure S2 indicates that the cut-off diameter value, expressed as optical equivalent, is 12 μm
6 for the AVIRAD inlet and 5 μm for the CAI.

7 To assess the impact of the inlets sampling efficiency on the measured optical properties, Mie
8 scattering calculations were performed to estimate n_r , n_i , ω_0 , g and k_{ext} using either the full size
9 distribution or the size distribution measured behind the aircraft inlets. For ω_0 , g and k_{ext} , we
10 considered a fixed refractive index of $1.52-0.003i$, reflective of the values observed for Saharan
11 dust in source region (Schladitz et al., 2009; Formenti et al., 2011a; Ryder et al., 2013a). The
12 discrepancies between ω_0 , g and k_{ext} , including or not larger particle sizes were used to estimate
13 the errors associated to the inlets sampling efficiency. For n_r and n_i , we estimated the difference
14 between \tilde{n} derived from the iterative procedure described above (i.e. Fig. 2) using the full size
15 distribution as input parameter and that obtained from the size distribution measured behind the
16 aircraft inlets. The absolute errors associated with ω_0 , g and k_{ext} due to the passing efficiencies
17 of the inlets were in the range covered by the measurements uncertainties of both optical
18 parameters and size distributions, which were estimated to be 0.02, 0.002, 0.04, 0.05 and 0.08,
19 respectively.

20

21 **2.4. Ancillary products**

22 Weather Research and Forecasting (WRF; Skamarock et al. 2008) simulations were performed
23 to investigate the meteorological conditions and the turbulence within the dust layers. The WRF
24 model is operational at the Department of Physics of the University of Genoa, Italy, in a three-
25 domain configuration. In particular, the simulations on the parent domain, covering the entire
26 Mediterranean basin with a horizontal grid spacing of 10 km, have been considered for the
27 present paper. Initial and boundary conditions were generated from the operational global
28 model GFS (Environmental Modeling Center, 2003) outputs (0.5×0.5 degree resolution). More
29 details about the modelling chain and the model setup are given in Bove et al. (2014), Cassola
30 et al. (2015), and Mentaschi et al. (2015).

31 As a complement, synoptic conditions and sea level pressure composite anomalies over the
32 Mediterranean basin during the campaign were analyzed using reanalysis data sets, such as the
33 NCEP/NCAR Reanalysis (Kalnay et al. 1996) and the NCEP Climate Forecast System (CFS)
34 reanalysis (Saha et al., 2010).

1 Source regions and atmospheric transport times of the dust plumes were determined through
2 the combination of satellite products and backward trajectories analysis. The potential source
3 regions active during the observational period were identified using the images from the
4 Spinning Enhanced Visible and Infrared Imager (SEVIRI) onboard the Meteosat Second
5 Generation (MSG) satellite. The NOAA HYbrid Single-Particle Lagrangian Integrated
6 Trajectory Model (HYSPLIT, <http://www.arl.noaa.gov/HYSPLIT.php>) using the Global Data
7 Assimilation System (GDAS) meteorological input was used to calculate whether an air mass
8 sampled by the aircraft could have originated from one of the identified active dust sources.
9 Backward trajectories were initialized using the time and the location when the aircraft
10 intercepted the air mass and were extended for up to 5 days prior the measurement. Backward
11 trajectory calculations were performed at the beginning, the middle and at the end of each SLR
12 to check the origin and transport pathway of the air masses through the measurements. We then
13 operationally define the dust age as the time elapsed since the calculated air mass trajectory
14 leave the ground where an active source was detected and the time of sampling by the aircraft.
15

16 **3. Results**

17 **3.1. Identification of the dust source region and transport pathway**

18 During the ADRIMED campaign, the synoptic situation was characterized by a “dipolar” sea
19 level pressure anomaly pattern, with positive anomalies in the western Mediterranean and
20 negative ones in the eastern part of the basin, as illustrated in Figure 4 (left panel). While this
21 situation induced stronger and more frequent than normal northwesterly winds over the Sardinia
22 and Sicily channels, the average conditions at mid-atmospheric levels during the campaign were
23 closer to climatological ones (Figure 4, right panel). Moulin et al. (1998) have documented the
24 frequency of dust episodes across the Mediterranean Sea, summer occurrences are quite
25 frequent.

26 The synoptic conditions during each of the 9 flights described in Figure 1 and Table 1 are
27 summarized in Figure S3 and S4 in the Supplementary Material, where sea level pressure and
28 500-hPa geopotential height are shown. A low-pressure system can be found over the Atlantic
29 on June 16, moving towards the Iberian Peninsula, while a subtropical ridge extends from North
30 Africa to Central Mediterranean. This situation induced a strong south-southwesterly flow,
31 firstly towards Southern Iberia and western Mediterranean (16-17 June), then extending
32 eastwards and reaching Corsica on the subsequent days, favouring dust transport from the
33 Saharan region. This is quite evident from Figure S5, showing 700-hPa wind and relative
34 humidity maps from the WRF model. Figure 1 shows the likely sources regions for dust

1 sampled during the flights, identified from HYSPLIT simulation and MSG-SEVIRI satellite
2 products. Mineral dust were most likely uplifted from southern Morocco and Southern Algeria
3 and were sampled during flights F29, F30, F31 and F32 after 3.5-4.5 days of transport.
4 On 19-20 June the remnants of the aforementioned low are still visible as an upper level trough
5 over the western Mediterranean (Figure S5), triggering meridional transport at higher levels
6 from North Algeria/Tunisia region towards the Sardinia and Sicily Channels. This is confirmed
7 by backward trajectory and satellite product analyses showing that the dust sampled during the
8 flight F33-34 travelled 1 to 5 days from North Algeria/Tunisia before their sampling (not
9 shown). On 28 June during flight F38, an upper level low is found over the Alps and Central
10 Europe, inducing a westerly flow from Tunisia where mineral dust were most likely uplifted
11 towards Sicily at 700 hPa (Figure S6), while the surface high pressure over East Atlantic and
12 Iberia is associated to northwesterly winds at lower levels throughout most of Central
13 Mediterranean. Finally, the situation during the last flight F42 (3 July) was characterized by a
14 modest depression over Iberia, while the Azores anticyclone extended towards the
15 Mediterranean. As a consequence, upper level winds were mainly southwesterly over North
16 Africa, veering to westerly or northwesterly over the Sardinia and Sicily Channel, thus
17 contributing to dust transport in the area. We estimate that mineral dust originating from South
18 Morocco and Tunisia was transported for 3.5 days before sampling.
19 The identification of the dust source regions was confirmed by the measurements of the
20 elemental composition. Overall, Si/Al ranged between 2.4-2.7 and Fe/Ca between 0.3-0.7 in
21 the samples collected during ADRIMED. This is consistent with values previously reported for
22 mineral dust originating from Algeria, Tunisia and Morocco (Scheuvens et al., 2013; Formenti
23 et al., 2014). The identified emission areas also correspond to known source regions such as the
24 Grand Erg occidental at the border between Algeria and Morocco, the Mekkeranne in Algeria
25 and the Chott El Jerid in Tunisia (Ginoux et al., 2012).

26

27 **3.2. Vertical distribution of mineral dust**

28 Figure 5 shows the vertical profiles of the aerosol scattering coefficient σ_{scat} at $\lambda = 450, 550$ and
29 700 nm, the total particle number concentration in the submicron (N_{fine} ; $5\text{nm} < D_p < 1 \mu\text{m}$) and
30 the supermicron (N_{coarse} ; $D_p > 1\mu\text{m}$) size ranges, and the vertical distribution of the scattering
31 Angstrom exponent \AA calculated between 450 and 770 nm. The top height of the boundary
32 layer (Z_b) and the wind shear level (Z_s) are also indicated in Figure 5 by a solid and a dashed
33 line, respectively. All the vertical profiles were characterized by a weak and positive gradient
34 of the potential temperature, characteristic of a stratified atmosphere (Figure S7). The top height

1 of the boundary layer was identified as the height at which the temperature profile showed the
2 highest discontinuity and the water vapor mixing ratio decreased the most rapidly. The shear
3 level was determined from the sudden increase in wind speed and change in wind direction
4 (Figure S7).

5 Mineral dust was observed above the boundary layer in layers extending from 1 km to more
6 than 6 km above sea level (asl) (Figure 5). The presence of mineral dust within the boundary
7 layer was not attested neither by chemical analyses nor with the back-trajectories analyses,
8 which revealed that in the 5 days prior sampling, low-level air masses originated from the
9 European continent or recirculated within Mediterranean basin. The transport of mineral dust
10 in the free troposphere up to 9 km in altitude is a common observation in the Mediterranean
11 region, as previously reported by lidar measurements (Dulac and Chazette, 2003; Gobbi et al.,
12 2000; Mona et al., 2006; Di Iorio et al., 2009; Gómez-Amo et al., 2011). Such high altitudes
13 may be linked to the strong vertical convective processes over the dust source regions, which
14 lift dust particles at high atmospheric levels (Flamant et al., 2007, Papayannis et al., 2008;
15 Cuesta et al., 2009).

16 The dust vertical structures showed an important variability. Complex and stratified structures
17 were observed depending on the position of Z_b and Z_s . During the campaign, the wind shear
18 level was equal to or higher than the top of the boundary layer.

19 When Z_s and Z_b coincided (F30, F31, F32, F38), the dust vertical structure was characterized
20 by a single and rather homogeneous layer. It is noteworthy that apparently similar thermo-
21 dynamical situations displayed a different spectral dependence of the scattering coefficient, as
22 for example is the case above the boundary layer for flights F32 ($\text{\AA} \sim 0.3$) and F38 ($\text{\AA} \sim 0.9$),
23 pointing out differences in the particle type. The values of \AA observed during the flight F38
24 were higher than the values of ~ 0.5 reported for Saharan dust in source region (McConnell et
25 al., 2008a; Muller et al., 2011b), but lower than values of $\text{\AA} > 1$ reported for air masses
26 dominated by pollution aerosols in the western Mediterranean basin (Di Biagio et al., 2015). It
27 is reasonable to suppose that the profile F38 reflects a situation where desert dust was mixed
28 with pollution particles. This is confirmed by the five-day backward trajectories (Figure 6a),
29 which indicates air parcel coming from Europe and traveling at least three days above the
30 Mediterranean Sea within the boundary level before its uplift over Tunisia.

31 When Z_s was higher than Z_b (F33, F34, F35), mineral dust was found in two distinct layers
32 below and above 3 km asl. The five-day backward trajectories suggest that these dust layers
33 originated from different dust source regions (Figure 1 and Table 1). An example is given by
34 the flight F35 (Figure 6b) for which the above-3km dust layer originated from central Algeria

1 and was carried by northern flow to Lampedusa in 3.5 days, whereas the below-3km dust layer
2 was transported from the southeastern Morocco-southwestern Algeria border region by a
3 westerly flow within 3 days. Similar structure with multilayering of the Saharan dust
4 corresponding to air masses from different dust source regions was previously observed by lidar
5 measurements in the Mediterranean region (Hamonou et al., 1999; Guerrero-Rascado et al.
6 2008).

7 Regardless of the thermo-dynamical structure of the atmosphere, the aerosol vertical profiles
8 revealed a clear vertical variability of the contribution of fine mode particles in the dust layers.
9 The values of N_{fine} and \dot{A} were generally below 1000 \# cm^{-3} and 0.5, respectively, in dust layers
10 above 3 km asl. In contrast, N_{fine} and \dot{A} were up to 4000 \# cm^{-3} and 2.2, respectively, in the dust
11 layers below 3 km altitude (Figure 5). These observations suggest that either the dust plumes
12 carried more fine particles during transport below 3 km altitude or dust particles in the fine
13 mode exhibited a vertical gradient.

15 **3.3. Size distribution of the dust plumes**

16 Particle number size distributions classified as a function of altitude are shown in Figure 7.
17 Table 3 presents the average characteristics of the parameterized four-modal number size
18 distributions.

19 In the fine mode, the size distributions showed three modes around 80, 120 and 320 nm (Figure
20 7a). For particles smaller than 300 nm, the shapes of the size distributions in the dust layer and
21 in the boundary layer were quite similar. As particles in this size range mostly reflect
22 anthropogenic influences from near or distant sources (Birmili et al., 2010), this indicates that
23 the pollution plumes from the surface were exported above the boundary layer and mixed with
24 the dust layers. The particle size distributions in the dust layers above 3 km followed a similar
25 pattern as in the dust layers below 3km but number concentrations 2 times smaller were
26 observed for the modes at 80 and 120 nm, suggesting that the concentration of pollution
27 particles varied with the altitude. For particles between 300 nm and $1 \mu\text{m}$, the particle size
28 distributions were reasonably constant for dust layers at various altitudes. Kaaden et al. (2008)
29 found dust particles as small as 300 nm diameter in Morocco, which was also confirmed by
30 Kandler et al. (2009). The decrease of N_{fine} with altitude (i.e. Figure 5) was therefore most likely
31 due to the larger concentration of sub-300 nm pollution particles transported in the dust plumes
32 below 3 km altitude. The fact that an identical median diameter $D_{p,g}$ was used to parameterize
33 the number size distributions in the fine mode for below- and above-3km layers (Table 3) and
34 the prevalence of a sub-300 nm particles in the below-3 km dust layer (Figure 7a) might also

1 reflect that the mixing between the pollution and the dust plumes was mostly external in the
2 fine mode.

3 In the coarse mode, a modal diameter of the number size distribution between 1.3 and 2.0 μm
4 was observed indiscriminate of dust altitude. This indicates that the dust layers transported over
5 the Mediterranean basin were well-mixed vertically in terms of coarse particle population, as
6 previously observed by Weinzierl et al. (2011) for mineral dust after short-range transport over
7 the eastern Atlantic Ocean. Conversely, the number concentration of large dust particles
8 decreased with increasing altitude for freshly uplifted Saharan dust (Weinzierl et al., 2009;
9 Ryder et al., 2013a). There are some evidences suggesting that the well-vertical mixing of the
10 dust plumes occurs during the first day following the dust uplifted (Ryder et al, 2013b).
11 Turbulent fluxes within the dust layer might be responsible for the vertical distribution of the
12 dust aerosols becoming more homogeneous in terms of coarse mode particles as the dust ages
13 (Rosenberg et al., 2014). Particles in the coarse mode showed a large flight-to-flight variability
14 with number concentrations varying by more than one order of magnitude. This is quite evident
15 in Figure 7b showing the conversion of number size distributions into volume size distributions.
16 This variation in concentration might reflect the wide range of dust event encountered during
17 the campaign in terms of source regions, time of transport and meteorological conditions.

18 The spread of volume size distributions obtained during ADRIMED overlaps with those
19 measured during other airborne campaigns close to dust source regions (AMMA, FENNEC and
20 SAMUM-1) in the coarse mode size range (Figure 7c). Effective diameters of the coarse mode
21 $D_{eff,c}$ (*i.e.* estimated in the size 1-32 μm as defined in eq. 7) ranged from 3.8 to 14.2 μm during
22 ADRIMED, which is in the range of magnitude of the mean values of 3.8, 8.8 and 7.4 μm
23 obtained during AMMA, FENNEC and SAMUM-1, respectively (Formenti et al., 2011b; Ryder
24 et al. 2013a; Weinzierl et al., 2011). Contrastingly, fewer particles larger than 10 μm were
25 counted after short-range transport over the eastern Atlantic Ocean in the Cape-Verde region
26 during SAMUM-2 with respect to the other campaigns. $D_{eff,c}$ around 3.2 μm was found in the
27 dust layers during SAMUM-2 (Weinzierl et al., 2011).

28

29 **3.4. Optical properties of the dust plumes**

30 Figure 8a-b shows the vertical distribution of the real and imaginary parts of the refractive index
31 \tilde{n} . Within the dust plumes, \tilde{n} ranged from 1.50 to 1.55 for the real part and remained below
32 0.005 for the imaginary part. Since \tilde{n} is related to the aerosol chemical composition (Liu and
33 Daum, 2008), it is expected to be influenced by the mixing rate of the dust plume with pollution
34 particles. We thus plotted the values of \tilde{n} as a function of the Angstrom exponent \mathring{A} . Besides

1 not displaying significant variation with the altitude, the values of \tilde{n} did not show any
2 dependence on \AA . The results obtained during ADRIMED have been compared with data in the
3 literature for Saharan dust in or near-sources in Figure 8. For both the real and imaginary parts,
4 our estimates of \tilde{n} fall within the range of variability (1.51 - 1.57 and 0.0001 - 0.0046 for the
5 real and the imaginary parts, respectively) documented in source regions (Schladitz et al., 2009;
6 Formenti et al., 2011a; Ryder et al., 2013b). This variability was attributed to the variability of
7 the mineralogical composition of dust originating from diverse source regions (Kandler et al.,
8 2009; Petzold et al., 2009). Our data do not show any clear dependence of \tilde{n} on dust source
9 region either (not shown), which is consistent with the limited regional variability of the dust
10 optical properties found 1-2 days after emissions in Africa by Formenti et al. (2014) from
11 aircraft measurements. This is probably a consequence of the mixing of dust from various active
12 sources occurring with each other during transport shortly after emission. A number of
13 uncertainties in our identification of dust source region is associated with the employed
14 methodology. The trajectory error associated with calculation of back trajectories from
15 HYSPLIT reaches 15–30 % of the travel distance (Draxler and Rolph, 2013). Another potential
16 source of uncertainty is the difficulty to discriminate the satellite aerosol signals from the
17 surface reflectance using MSG-SEVIRI observations, especially over bright surfaces (Kutuzov
18 et al., 2013). Moreover, even if the origin of the air masses was checked at the beginning, the
19 middle and at the end of each straight-levelled runs, larger number of sources could potentially
20 contribute to the aircraft samples because of aircraft's movements during sampling.

21 The vertical distribution of intensive optical properties relevant to radiative transfer (i.e. single
22 scattering albedo ω_0 , asymmetry parameter g and extinction mass efficiency k_{ext}) are shown in
23 Figure 8c-e and Table 4. Estimates of ω_0 , g and k_{ext} fall within the range 0.90 - 1.00, 0.6 - 0.8
24 and 0.2 - 0.7 $\text{m}^2 \text{g}^{-1}$, respectively. Overall, there is not clear dependence on the altitude. Only
25 slightly low values of g (from ~ 0.7 to ~ 0.8) and k_{ext} (from ~ 0.2 to $\sim 0.7 \text{m}^2 \text{g}^{-1}$) were observed
26 for some dust layers below 3 km asl. As \tilde{n} was found to be constant with the altitude (i.e. Figure
27 8a-b), these variations in g and k_{ext} were probably due to the variability in particles size
28 distributions, which is consistent with the larger fraction of fine particles found in the higher
29 altitude dust layers (i.e. Figure 7a). Values of ω_0 , g and k_{ext} remained, however, within the range
30 of values reported in source regions by Schladitz et al. (2009), Formenti et al., (2011a) and
31 Ryder et al., (2013b). Despite the fact that dust plumes carried pollution particles during their
32 long-range transport in the Mediterranean region, the dust optical properties appeared to be
33 unaffected by this mixing.

1 In the Mediterranean region, previous estimates of ω_0 for dust particles were obtained from
2 remote-sensing techniques. Mallet et al. (2013) reported from multi-year ground-based
3 AERONET observations a column-averaged ω_0 of 0.92-0.95 between 440-880 nm for various
4 sites over the Mediterranean under the influence of dust aerosols. Using a similar approach, Di
5 Biagio et al. (2009) reported lower column-averaged ω_0 values during dust transport events
6 when boundary-layer air masses are transported from central Europe, probably rich in absorbing
7 particles from urban-industrial European areas. Values as low as 0.88 at 530 nm were also
8 determined by Sicard et al. (2012) during a case study of a dust plume transported over
9 Barcelona and accompanied by a biomass-burning outbreak. Recently, Valenzuela et al. (2014)
10 presented eight months of dust optical properties over the Alborán Island from Sun photometer
11 measurements for dust plumes originating from northwestern Africa and passing over several
12 urban-industrial areas along the coast of Morocco and from eastern Africa and traveling over
13 the Mediterranean Sea. No significant changes in column-averaged ω_0 were reported for the
14 different air masses, which indicates that the influence of anthropogenic fine particles
15 originating from the urban-industrial areas in the north of Africa during desert dust outbreaks
16 was negligible. Overall, these contrasting results highlight the major role of the transport
17 conditions (height, air mass encountered) of the dust plumes in governing the mixing processes
18 of mineral dust with other aerosol species.

19

20 **4. Discussion**

21 **4.1. On the role of transport conditions in the mixing of pollution particles with** 22 **mineral dust**

23 In this section, we investigate the transport conditions of the dust layers expected to influence
24 the mixing of mineral dust with pollution particles. As previously mentioned, the highest
25 concentrations of pollution particles were detected in the below-3km dust layers. We further
26 investigate this result by examining the variations of $D_{eff,f}$ and $D_{eff,c}$ with the altitude of the dust
27 plumes. We assume that changes in $D_{eff,f}$ reflected different fractions of externally mixed
28 pollution particles smaller than 300 nm in the dust plumes, as discussed in section 3.3. In Figure
29 9a, a sharp transition in the proportion of fine particles can be seen in $D_{eff,f}$ at 3 km asl. with
30 greater proportion of pollution particles found in the lower 3 km of the atmosphere. The
31 observation of pollution particles at altitudes up to 3 km during ADRIMED is comparable with
32 the average height of pollution layers observed in the western Mediterranean basin (Meloni et
33 al., 2003; Mallet et al., 2005; Junkermann et al., 2009; Di Biagio et al., 2015). Hence, the
34 vertical extent of pollution particles might explain the fact that the below-3km dust plumes were

1 more affected by fine particles than the above-3km dust layer. The coarse mode of the dust
2 plume is also expected to be impacted by the presence of pollution particles. In case of an
3 internal mixing between pollution particles and mineral dust, the mean particles size should
4 increase. During ADRIMED, $D_{eff,c}$ of the dust plume did not show any systematic dependence
5 on altitude (Figure 9b). This finding must however be interpreted with some caution since $D_{eff,c}$
6 was affected by the large uncertainties in FSSP-300 and GRIMM sizing (i.e. section 2.2.1.) that
7 might hide the detection of small aggregates on dust.

8 The mixing extent of pollution particles in dust layers is also expected to depend on the transport
9 time of the plumes. Figure 10 shows $D_{eff,f}$ against the estimated age of the dust air mass and
10 divided according to the height of transport of the dust plumes. From these measurements, we
11 do not find significant trend in the dust mixing rate with transport time in both below- and
12 above-3km layers. This result is not surprising for the above-3km dust layers since we found
13 that the interaction of dust plumes with pollution particles was limited when they were
14 transported above 3 km asl. For dust plumes below 3 km asl., their transport time was at least
15 3 days before sampling during ADRIMED. Afterwards the dust spent time over pollution
16 regions appeared to have no more effect on the mixing extent of pollution particles. The
17 constant $D_{eff,f}$ values observed within the below-3km dust plumes and the boundary layer
18 (Figure 9a) suggests also that the vertical transport and mixing of pollution particles with dust
19 plumes were already completed at the time of sampling. Note that the below-3km dust layers
20 reached the Mediterranean coasts affected by urban/industrial emissions after having undergone
21 around 2 days of transport. Hence, the pollution mixing rate appears to be a relatively rapid
22 process more likely driven by the height of transport of the dust layers.

23

24 **4.2. Contribution of pollution particles to the absorption properties of the dust** 25 **plumes**

26 We evaluated the effect of the contribution of pollution particles to the absorption properties of
27 the dust layers by calculating ω_0 from the mass concentration of the main anthropogenic
28 compounds. Table 5 shows the mass concentration of major elements, ionic species and rBC
29 measured in the dust plumes. The dust mass concentration estimated from the measured Al
30 using the mean Al mass fraction in the crustal composition of 7.09% (Guieu et al., 2002) is
31 also shown. In all samples, silicates were the most abundant type of dust particles, as expected
32 from previous chemical analysis of dust in North Africa (Scheuven et al., 2013; Formenti et
33 al., 2014). The presence of pollution particles within the dust plumes is confirmed by the

1 detection of SO_4^{2-} and rBC as well as typical anthropogenic trace elements such as V, Pb and
2 Zn.

3 SO_4^{2-} reached concentrations typical of the Mediterranean region in summertime (Ripoll et al.,
4 2015) with the largest concentration of $2.5 \mu\text{g m}^{-3}$ found over Corsica during the flight F34. The
5 positive correlation between the concentration of SO_4^{2-} and N_{fine} indicates the presence of
6 externally mixed sulfate-containing particles in the fine mode particles, such as ammonium
7 sulfate particles. $\text{SO}_4^{2-}/\text{NH}_4^+$ ratios being higher than unity, the presence of SO_4^{2-} in the dust
8 layers can also either be due to nucleation of sulfuric acid in polluted plumes, or to sulphate
9 formation at the surface of preexistent particles by uptake of gaseous sulfur dioxide or by
10 coagulation of sulphate particles (Ullerstam et al., 2002; Korhonen et al., 2003; Sullivan et al.,
11 2009).

12 Concentrations of rBC ranged from 0.04 to $0.13 \mu\text{g m}^{-3}$. Although these values are much lower
13 than concentrations measured in areas of high industrial or traffic density (Liu et al., 2014;
14 Mantas et al., 2014), they are in agreement with concentrations found in continental and
15 background area of the western Mediterranean (Ripoll et al., 2015). Except in the case of large
16 forest fires, rBC concentrations are generally low on average in summertime due to the absence
17 of the major sources of emission, such as domestic wood burning (Tsyro et al., 2007).

18 Calculations of ω_0 from the aerosol chemical composition were performed assuming that dust
19 was externally mixed with rBC and sulfate. Indeed, prevalence of an external mixing between
20 dust particles and rBC has been observed from long-term measurements in the western
21 Mediterranean basin (Ripoll et al., 2015). Moreover, coating of sulfate on mineral dust has been
22 shown to have no significant effect on dust optical properties (Bauer et al., 2007). Calculations
23 of ω_0 were performed as follows:

$$\omega_0 = \frac{\sum_i (k_{ext,i} - k_{abs,i}) \cdot C_{m,i}}{\sum_i k_{ext,i} \cdot C_{m,i}} \quad (9)$$

24 We used mean mass absorption and extinction efficiencies (i.e. the total light absorption or
25 extinction per unit mass of aerosol, referred as k_{abs} and k_{ext}) of $0.02 \text{ m}^2 \text{ g}^{-1}$ and $0.64 \text{ m}^2 \text{ g}^{-1}$ for
26 dust (Hess et al., 1998), $7.5 \text{ m}^2 \text{ g}^{-1}$ and $9.4 \text{ m}^2 \text{ g}^{-1}$ for rBC (Bond and Bergstrom, 2006) and 0 m^2
27 g^{-1} and $5.0 \text{ m}^2 \text{ g}^{-1}$ for sulfate (Charlson et al., 1992). As shown in Table 5, ω_0 obtained from this
28 calculation ranged from 0.93-0.97, which falls within the range of values obtained from
29 measurements ($0.92\text{-}0.99 \pm 0.04$). For comparison, we estimate that ω_0 for pure mineral dust
30 was 0.97. This simple approach confirms the small influence of pollution particles on the optical
31 properties of the dust plumes over the Mediterranean region.

1 The ADRIMED field campaign was characterized by moderate AOD with averaged values
2 ranging between 0.1 – 0.6 at 440 nm as observed by AERONET/PHOTONS sun-photometers
3 (see Figure 19 of Mallet et al., 2015). Outside of dust events, the AOD displayed values from
4 0.1 to 0.2 (440 nm), while it reached values up to 0.8 under dusty conditions. Although higher
5 AOD values have already been observed in the Mediterranean region during intense pollution
6 or biomass burning events (Pace et al., 2005; Alados-Arbodelas et al., 2008; Péré et al., 2011),
7 values obtained during ADRIMED are typical of those observed in summertime (Nabat et al.,
8 2015). This observation is also supported by the mass concentration of the main anthropogenic
9 compounds that reached typical values for the region, as discussed previously. Our result on the
10 moderate absorption properties of the dust plumes is thus likely relevant to dust events in the
11 western Mediterranean in the absence of intense pollution or biomass burning emissions and
12 can be used for constraining modeling studies and satellite retrievals that make assumption on
13 dust optical properties.

14 We compared our measurements on dust absorption properties with values published in the
15 OPAC aerosol database that is widely used by modelling and remote sensing communities. The
16 result of this comparison indicates an overestimation of dust absorption properties in the OPAC
17 database. The n_i value achieved in the OPAC database ($n_i=0.006$) are high compared to values
18 observed for Saharan mineral dust in source region and over the Mediterranean during
19 ADRIMED (n_i between 0.000–0.005). This finding is in line with previous studies showing
20 disagreements in dust absorption between satellite retrievals and modelling studies that has been
21 solved by decreasing the imaginary part of the dust refractive index (Kaufman et al, 2001;
22 Moulin et al, 2001; Balkanski et al., 2007; Mian Chin et al., 2009).

23

24 **4.3. Retention of coarse mode particles in the dust plumes**

25 Figure 11 shows $D_{eff,c}$ against the estimated age of the dust air mass. Observations from aircraft
26 during previous campaigns are shown for comparison. The $D_{eff,c}$ values did not change with
27 time, suggesting that the dust layers transported over the Mediterranean region tend to conserve
28 their coarse mode with time. During ADRIMED, $D_{eff,c}$ values obtained in dust layers having
29 spent less than 1.5 days in the atmosphere are consistent with those obtained near dust source
30 regions (Formenti et al, 2011b; Weinzierl et al., 2011). Conversely, dust layers having spent
31 more than 1.5 days in the atmosphere present higher $D_{eff,c}$ than previously observed over the
32 Atlantic ocean (Maring et al., 2003; Weinzierl et al., 2011). The loss of large dust particles after
33 transport as observed over the Atlantic Ocean is most likely associated to the removal processes
34 occurring as the dust travels downwind (Mahowald et al., 2014). As smaller particles fall

1 downward much slower than larger particles, coarse particles are expected to be more prevalent
2 close to the sources regions. To date only few studies have focused on understanding the
3 evolution of dust size distribution, especially during transport over the Atlantic Ocean (Maring
4 et al., 2003; Reid et al., 2003; Kalashnikova and Kahn, 2008). These measurements pointed out
5 large differences between the observed and modeled evolution of dust size, with a lifetime of
6 coarse particles longer than expected from deposition theories. This suggests that other
7 processes counterbalanced the loss of large particles by dry deposition along transport. These
8 processes seem to be particularly important in the Mediterranean region, since the proportional
9 volume of coarse particles in the size distribution did not vary substantially even after 5 days
10 of transport.

11 The persistence of coarse particles over the Mediterranean basin during transport could be
12 explained by the presence of temperature inversions in the middle troposphere keeping the dust
13 layers confined due to the stable stratification. This was revealed by most of the aircraft
14 temperature profiles (Figure S7). Furthermore, the WRF model simulations of the vertical
15 velocity and vertical cross-section indicate the existence of updraft/downdraft due to the
16 thermal turbulence within the dust layers circulating over the Mediterranean basin in
17 summertime, due to elevated temperatures within the dust layers and large insolation. An
18 example for flight F33 in the Corsica region is shown in Figure 12, where the vertical velocity
19 showed updrafts and downdrafts up to 0.5 Pa s^{-1} , corresponding to about 5 cm s^{-1} . This value is
20 at least one order of magnitude greater than the gravitational settling velocity (0.25 cm s^{-1})
21 expected for particles of $8 \mu\text{m}$ diameter, value indicated by Maring et al. (2003) as the threshold
22 above which sensible changes in dust size distribution during atmospheric transport across the
23 Atlantic could be observed. The occurrence of turbulent updraft and downdraft motion could
24 therefore result in an enhancement of the particle lifetime in the atmosphere over the
25 Mediterranean basin.

26

27 **5. Conclusions**

28 We presented the first *in situ* aircraft measurements of the size distribution and optical
29 properties of Saharan dust transported over the western Mediterranean basin within the
30 framework of the ADRIMED airborne campaign in June-July 2013. Dust particles originating
31 from Algeria, Tunisia and Morocco were sampled in the western Mediterranean basin after 1
32 to 5 days of transport from the source regions.

33 Measurements of aerosol vertical profiles revealed that dust particles were transported inside
34 well-defined layers above the boundary layer ($>1 \text{ km asl.}$) dominated by pollution and marine

1 particles. The dust vertical structure was extremely variable and characterized either by a single
2 layer or a more complex and stratified structure. Backward trajectories indicated that the
3 multilayering of the Saharan dust corresponded to air masses originating from different dust
4 source regions. Abundance of sub-300 nm particles in the Saharan dust layers suggested a
5 strong mixing of dust with pollution particles. The height of transport of the dust layers
6 appeared to be the main factor affecting the mixing extent of pollution particles with mineral
7 dust. Measurements showed higher concentration of pollution particles in dust layers below 3
8 km asl. than at higher altitude, resulting in scattering Angstrom exponent up to 2.2 below 3 km
9 asl. This coincides with the typical height of pollution layers (~3 km asl.) observed in the
10 western Mediterranean basin.

11 The optical properties of the dust layers were not significantly affected by this mixing with
12 respect to values reported for native dust. Mineral dust aerosols were found to be moderately
13 absorbing with values of ω_0 between 0.90 and 1.00 at 530 nm. Concurrent optical calculations
14 from the aerosol chemical composition revealed that the contribution of pollution particles to
15 absorption properties of the dust plumes was negligible. This was most likely due to the low
16 contribution of rBC (~2% in mass) in regards to the fraction of dust (~84%) and sulfate (~14%)
17 in the dust plumes. The concentrations of anthropogenic particles being typical of those
18 observed in the Mediterranean region in summertime, these results demonstrate that outside
19 severe episode of pollution or biomass burning, mineral dust dominate the optical properties of
20 the dust plumes in the Mediterranean even if source of pollution particles are present.

21 An important question for the dust direct, semi-direct and indirect radiative effects is how long
22 the coarse mode of dust particles is conserved during transport. We showed that the coarse
23 mode was conserved even after 5 days of transport in the Mediterranean, which contrasts with
24 the gravitational depletion of large dust particles observed during the transport of dust over the
25 Atlantic Ocean. The global importance of this result is however still linked to whether these
26 observations are ubiquitous or occur only for specific dust transport events. Dust events
27 differing in terms of source region, time and height for transport were reported in this study.
28 For all these case studies, the coarse mode of dust particles was conserved during transport,
29 which might reflect the representativeness of the situation mostly occurring in summertime in
30 the western Mediterranean basin.

31 Most climate models simulate currently the dry deposition as a positive relationship of the
32 particles size, leading in an underestimation of the fraction of coarse particles being transported
33 long distances (Mahowald et al., 2014). Given the scarcity of field studies investigating the
34 evolution of the dust size distribution during transport, our results point out key processes

1 controlling the retention of large dust aerosols. In particular, WRF model simulations
2 highlighted a strong turbulence within the dust layer with vertical velocity at least one order of
3 magnitude greater than the particle gravitational settling velocity. Particles could therefore
4 remain trapped in the atmosphere by this strong turbulence. Further studies involving a deep
5 analysis of aircraft measurements of turbulence parameters both in the Mediterranean and in
6 other geographical areas such as the Atlantic region are required in order to quantitatively
7 characterize this process and improve the representativeness of the temporal evolution of dust
8 size distribution in climate models useful for radiative impact or marine biogeochemical
9 applications.

10 The dataset obtained during the ADRIMED airborne campaign can also be used for
11 constraining satellite retrievals that make assumptions on dust properties in order to derive
12 water vapor profiles, surface temperatures and greenhouse gases concentrations. The results
13 presented here suggest that the size and optical properties of the dust plumes could be
14 assimilated to those of native dust in satellite retrievals in the western Mediterranean. A
15 straightforward comparison of our results with values published in the OPAC aerosol database,
16 which is widely used by the remote sensing communities, suggests that the OPAC database
17 overestimate dust absorption. Moreover, this important dataset provides opportunities for
18 evaluating satellite aerosol products (size, absorption properties, vertical profiles) over the
19 Mediterranean through comparison with our in-situ airborne measurements.

20 In terms of significance for direct and semi-direct radiative effects, the presence of moderately
21 absorbing particles within the dust layers can induce important modifications in the
22 tropospheric heating and surface cooling by perturbing the incoming and outgoing radiations.
23 Evidence for retention of coarse mode particles in the dust layers indicates also that mineral
24 dust may still be a significant source of cloud condensation nuclei and ice nuclei despite having
25 undergone long-range transport. Hence, mineral dust may have potentially important
26 implications for the regional climate and the rainfall patterns in the west Mediterranean that
27 should be quantitatively addressed in future modelling studies.

28

29 **Acknowledgements**

30 This research work has been supported by the French National Research Agency (ANR)
31 through the ADRIMED program (contract ANR-11-BS56-0006). This work is part of the
32 ChArMEx project supported by CNRS-INSU, ADEME, Météo-France and CEA in the
33 framework of the multidisciplinary program MISTRALS (Mediterranean Integrated Studies at
34 Regional And Local Scales; <http://mistrals-home.org/>). The aircraft deployment was also

1 supported by CNES. We thank the instrument scientists, pilots and ground crew of SAFIRE for
2 facilitating the instrument integration and conducting flying operations. We acknowledge Pierre
3 Nabat and the ENM students, especially Damien Serça, Jonathan Guth and Valentin Seigner
4 for their meteorological forecasts during the campaign. We thank the NOAA Air Resources
5 Laboratory (ARL) for the provision of the HYSPLIT transport and dispersion model used in
6 this study. We gratefully acknowledge the two anonymous reviewers whose suggestions helped
7 improve and clarify this manuscript.

8

1 Table 1: Detailed information about the flights (number (ID), date, take-off time (TO), landing
2 time (L) and route), the vertical profiles (latitude (Lat), longitude (Lon) and start time) and the
3 dust layers sampled (height in meter, origin, age in day) during the ADRIMED airborne
4 campaign. Times are expressed in Coordinated Universal Time (UTC).
5

Flight information					Vertical profile			Dust layer		
ID	Date	TO	L	Flight route	Lat	Lon	Start time	Height	Origin	Age
F29	16 June 2013	08:18	10:20	Cagliari - Minorca	40N	5E	09:50	2200-4500	southwestern Algeria	4.5
F30	16 June 2013	11:58	14:40	Minorca - Granada	37N	4W	14:20	2400-4800	southwestern Algeria	4
F31	17 June 2013	07:15	09:54	Granada - Minorca	37N	4W	07:15	2800-5400	southern Algeria	3.5
F32	17 June 2013	11:45	13:43	Minorca - Cagliari	40N	5E	11:45	1000-4600	southwestern Algeria	4.5
F33	19 June 2013	11:35	15:00	Cagliari - East Corsica	43N	9E	12:50	3000-4000	northeastern Algeria	2
								1500-3000	northeastern Algeria	3
F34	20 June 2013	11:00	14:15	Cagliari - West Corsica	43N	7E	12:20	>2800	Tunisia	1
								1600-2800	Tunisia	5
F35	22 June 2013	08:47	11:26	Cagliari - Lampedusa	36N	13E	10:25	>3500	southern Algeria	2
								1500-3500	southern Morocco	4
F38	28 June 2013	10:59	13:29	Cagliari - Lampedusa	36N	13E	12:30	1200-4500	Tunisia	3
F42	03 July 2013	08:29	11:55	Cagliari - Lampedusa	36N	13E	09:50	>3000	Tunisia	3.5
								<3000	southern Morocco	3.5

6
7

1 Table 2: Instruments detailed in this article operating onboard the ATR-42 aircraft during the
 2 ADRIMED campaign.
 3

Parameter measured	Instrument	Abbreviation	Location in the aircraft	Wavelength (nm)	Nominal size range (μm)	Temporal resolution
Size distribution	Forward Scattering Spectrometer Probe, Model 300, Particle Measuring Systems	FSSP-300	wing-mounted	632.8	0.28 - 20	1 s
	Ultra High Sensitivity Aerosol Spectrometer, Droplet Measurement Technologies	UHSAS	wing-mounted	1054	0.04 - 1	1 s
	Sky-Optical Particle Counter, Model 1.129, Grimm Technik	GRIMM	AVIRAD inlet	655	0.25 - 32	6 s
	Scanning mobility particle sizer, custom-built (Villani et al., 2007)	SMPS	community aerosol inlet	n/a	0.03 - 0.4	2 min
Integrated number concentration	Condensation Particle Counters, Model 3075, TSI	CPC	AVIRAD inlet	n/a	> 0.005	1 s
Chemical composition	Filter sampling	n/a	AVIRAD inlet	n/a	n/a	20-40 min
	Single particle soot photometer, Droplet Measurement Technologies	SP2	community aerosol inlet	1064	0.08 - 0.5	1 s
Scattering coefficient	3λ Integrated Nephelometer, Model 3563, TSI	Nephelometer	AVIRAD inlet	450, 550, 700	n/a	1 s
Extinction coefficient	Cavity Attenuated Phase Shift, Aerodyne Research Inc.	CAPS	community aerosol inlet	530	n/a	1 s

4
 5
 6

1 Table 3: Parameters (geometric median diameter $D_{p,g,i}$ in μm , standard deviation σ_i , and
 2 integrated number concentration $N_{tot,i}$ in $\# \text{cm}^{-3}$) of the four log-normal distributions used to
 3 parameterize the number size distributions obtained at the different altitudes. The mean,
 4 minimum and maximum of all parameters are listed.

5

		$D_{p,g,1}$	σ_1	$N_{tot,1}$	$D_{p,g,2}$	σ_2	$N_{tot,2}$	$D_{p,g,3}$	σ_3	$N_{tot,3}$	$D_{p,g,4}$	σ_4	$N_{tot,4}$
Above-3km dust layer	mean	0.08	1.25	170	0.12	1.60	300	0.32	1.70	15	1.3	2.2	3.0
	min	0.09	1.20	80.0	0.13	1.30	80.0	0.18	1.65	40	2.5	1.8	0.1
	max	0.08	1.25	320	0.12	1.56	600	0.32	1.70	45	1.3	2.2	12
Below-3km dust layer	mean	0.08	1.25	300	0.12	1.60	700	0.32	1.70	15	2.0	2.4	1.0
	min	0.08	1.25	250	0.11	1.50	400	0.20	1.70	35	1.7	2.1	0.7
	max	0.08	1.25	600	0.13	1.50	1100	0.18	1.90	80	1.7	2.0	2.5
Boundary layer	mean	0.08	1.25	450	0.12	1.60	650	0.32	1.70	5.0	1.3	2.1	1.0
	min	0.08	1.25	150	0.12	1.60	200	0.30	1.70	1.8	1.0	2.1	0.1
	max	0.08	1.25	600	0.12	1.60	1400	0.32	1.70	15	1.3	2.1	3.0

6
 7
 8
 9

1 Table 4: Optical parameters (real part of the complex refractive index n_r , imaginary part of the
 2 complex refractive index n_i , single scattering albedo ω_0 , asymmetry parameter g and mass
 3 extinction efficiency k_{ext}) all at $\lambda=530$ nm as a function of the altitude. The mean, minimum and
 4 maximum of all parameters are listed.

5

		n_r	n_i	ω_0	g	k_{ext}
Above-3km dust layer	mean	1.53	0.003	0.95	0.8	0.4
	min	1.50	0.000	0.90	0.7	0.3
	max	1.55	0.005	1.00	0.8	0.5
Below-3km dust layer	mean	1.52	0.003	0.94	0.7	0.5
	min	1.50	0.000	0.90	0.6	0.4
	max	1.55	0.005	1.00	0.7	0.7

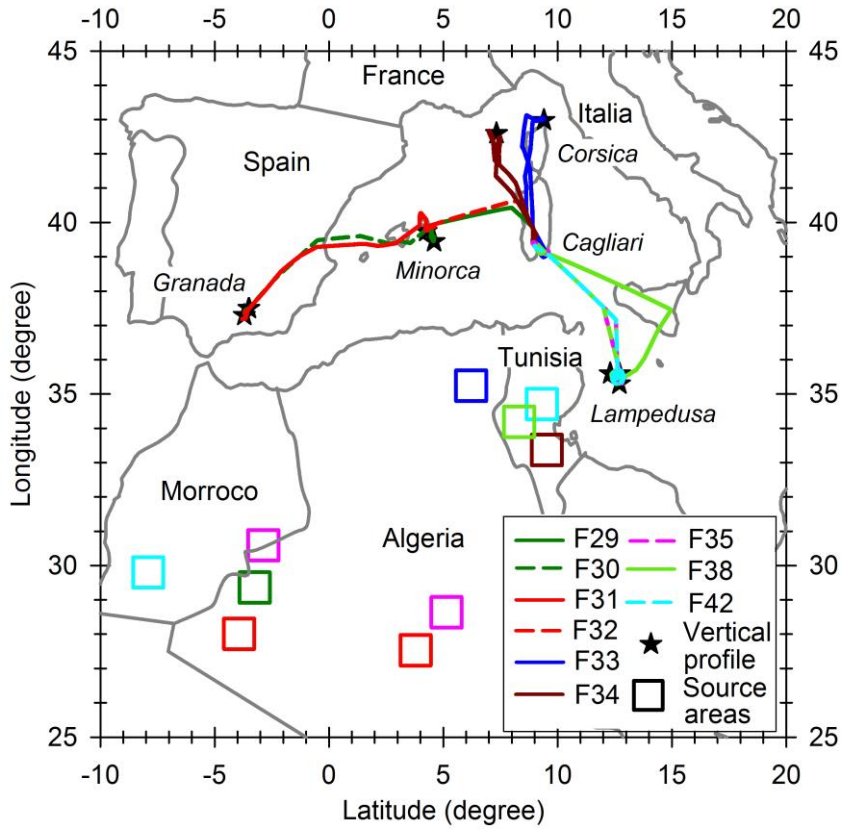
6

1 Table 5: Concentrations of major crustal (Si, Al, Fe and Ca, in ng m^{-3}) and metallic tracers (Si,
2 V, Pb and Zn, in ng m^{-3}), ionic species (SO_4^{2-} , NO_3^{2-} , NH_4^+ , in ng m^{-3}), black carbon (in ng m^{-3})
3 3), mineral dust (in $\mu\text{g m}^{-3}$) and integrated fine mode of particles (in $\# \text{cm}^{-3}$) during the
4 ADRIMED airborne campaign. Dash indicates that the specie concentration was lower than the
5 detection limit. The dust mass concentration was estimated from the measured Al using the
6 mean Al mass fraction in the crustal composition of 7.09 % (Guieu et al., 2002). A comparison
7 of the single scattering albedos ω_0 measured by the nephelometer and CAPS with those
8 estimated from chemical measurements is also shown. The absolute error associated with ω_0
9 obtained from measurements is 0.04.
10

Flight number	F29	F30	F31	F32	F33	F34	F35	F38	F42
Si	3607	4955	4159	592	2426	9814	6430	2040	5366
Al	1404	2028	1719	225	975	3770	2519	746	2146
Fe	687	1085	845	146	536	1869	1239	416	1032
Ca	1099	1596	1547	-	1322	6404	2112	1374	1592
V	9	6	5	17	16	22	19	13	-
Pb	82	458	28	216	417	-	762	-	-
Zn	20	34	25	4	-	-	71	-	-
SO_4^{2-}	-	1740	-	2016	1574	2505	966	1764	2011
NO_3^-	-	-	-	206	-	285	309	-	467
NH_4^+	-	809	276	640	563	613	-	557	-
rBC	62	97	64	130	57	97	37	97	78
Dust	15.1	21.7	18.4	2.4	10.5	40.5	27.0	8.0	23.0
N_{fine}	316	416	457	881	515	988	229	485	714
ω_0 (measured)	0.97	1.00	0.99	0.92	0.98	0.94	0.97	0.94	0.99
ω_0 (chemistry)	0.93	0.96	0.95	0.94	0.96	0.96	0.97	0.94	0.96

11

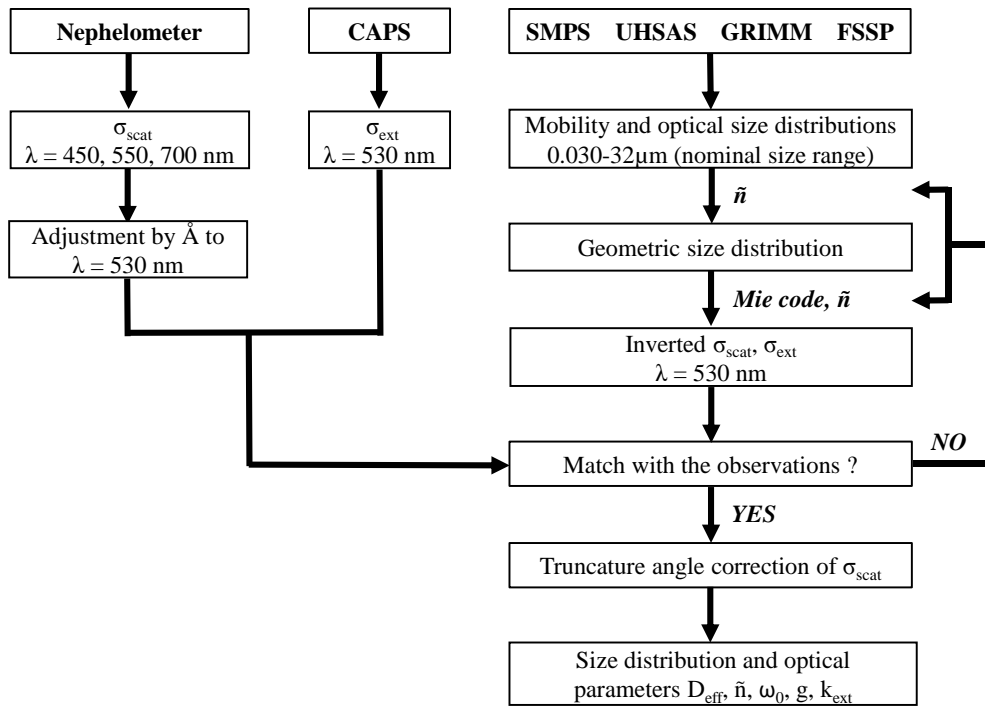
1 Figure 1. Operating region of the ATR-42 aircraft during the ADRIMED flights that performed
 2 mineral dust measurements. Colors of the lines and squares correspond to the different flights.
 3 The positions of the middle of the profiles are shown in black stars. Squares indicate likely
 4 sources regions of the dust sampled during the flights. The aircraft was based at Cagliari in
 5 Sardinia.



6
7

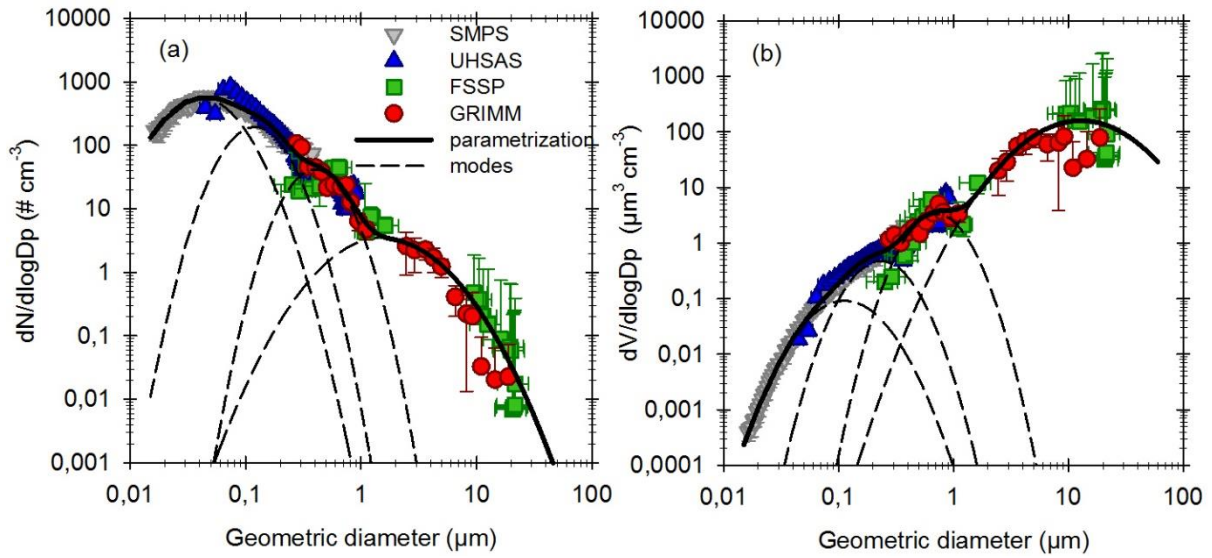
1 Figure 2: Data inversion procedure to retrieve the dust size distribution and optical parameters.

2



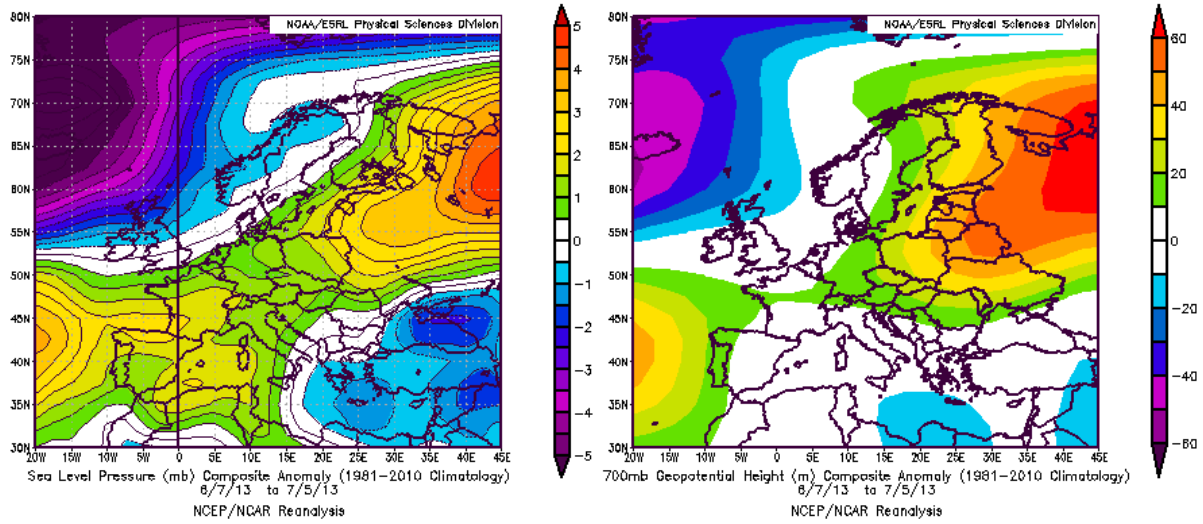
3

1 Figure 3. Number (a) and volume (b) size distributions obtained by the SMPS (gray), UHSAS
 2 (blue), FSSP (green) and GRIMM (red) during the flight F35 including refractive index
 3 corrections for $\tilde{n} = 1.53 - 0.004i$. Vertical errors bars indicate one standard deviation of the data
 4 during the straight levelled run. Horizontal errors bars display the bin sizing uncertainties of the
 5 instruments. The dark line represents the parametrized fit with a sum of four log-normal modes
 6 (shown in dashed lines).



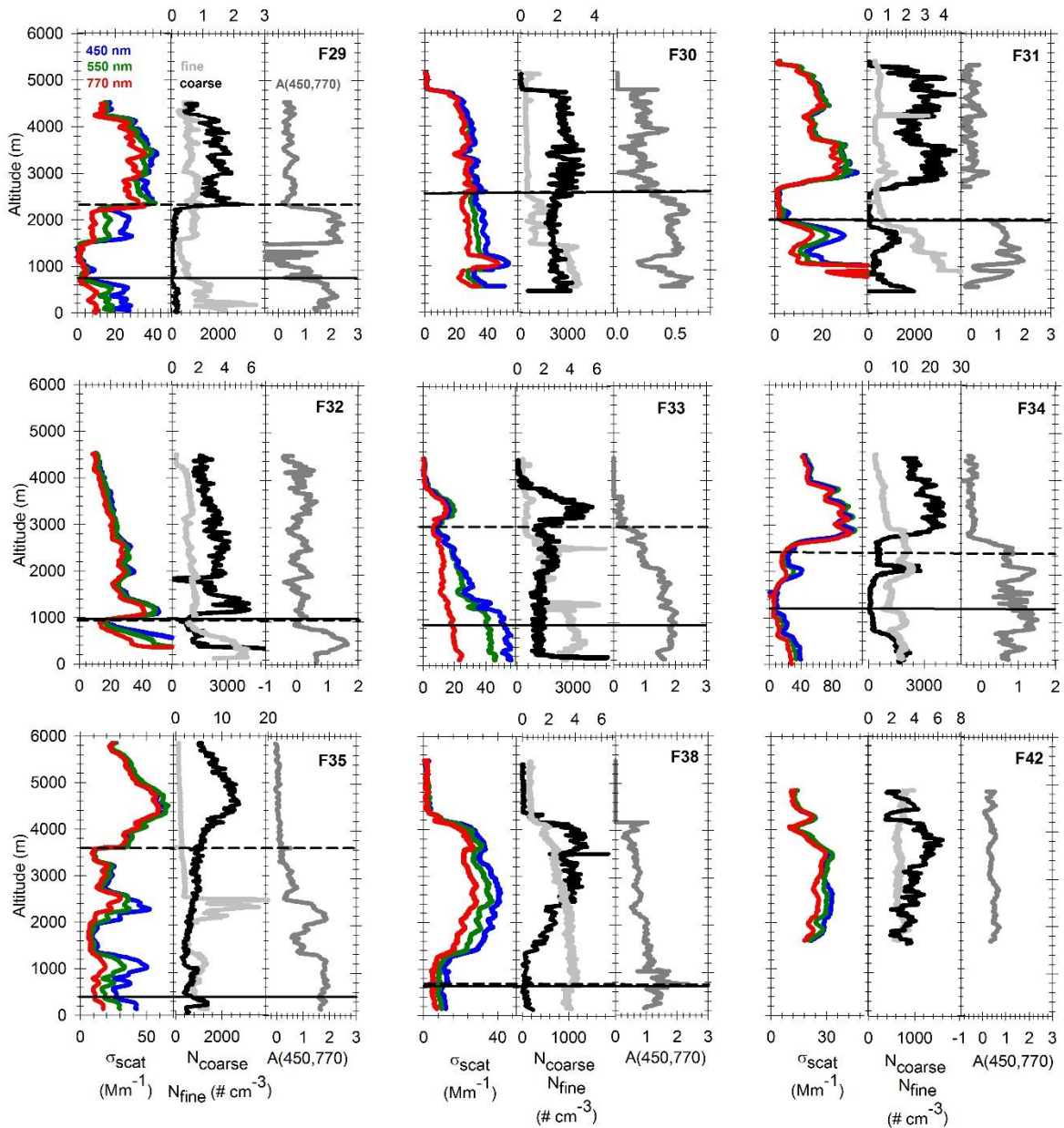
7
 8
 9
 10

1 Fig. 4. Sea level pressure in hPa (left) and 700 hPa geopotential height in m (right) composite
 2 anomalies with respect to the 1981-2010 climatology obtained from the NCEP/NCAR
 3 Reanalysis (images provided by the NOAA/ESRL Physical Sciences Division, Boulder
 4 Colorado, from their web site at <http://www.esrl.noaa.gov/psd/>).
 5



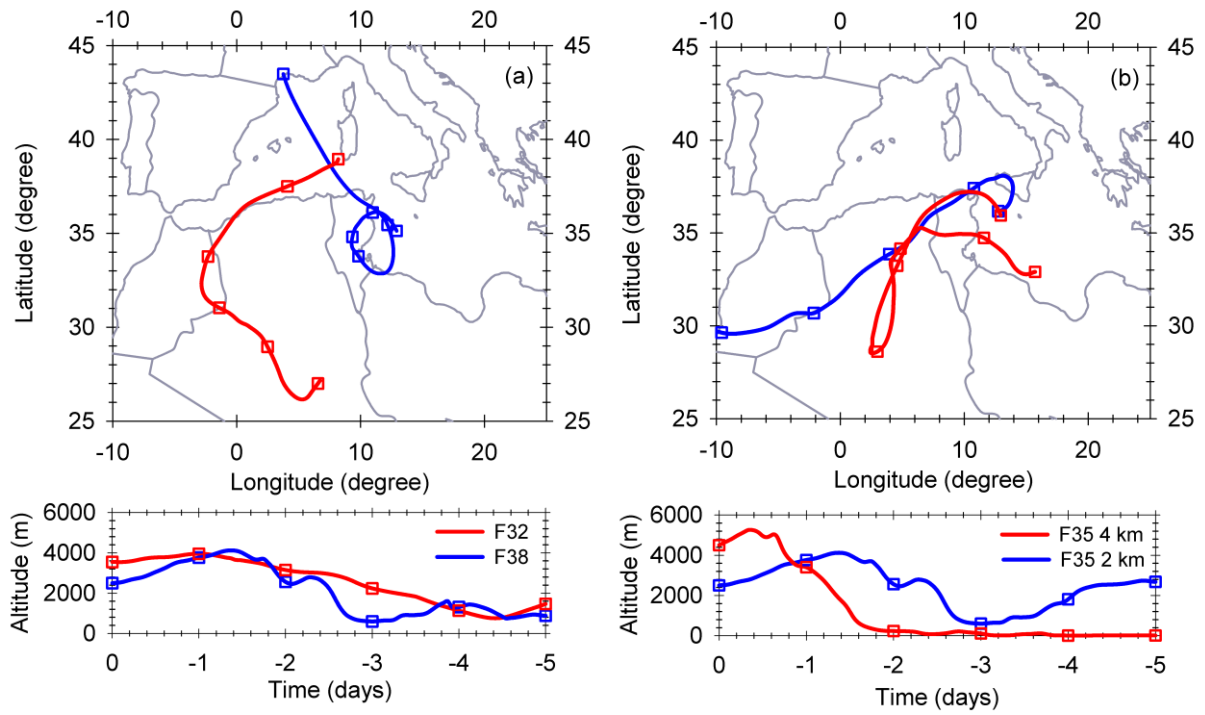
6
7

1 Figure 5. Vertical profiles of the spectral scattering coefficient σ_{scat} at $\lambda=450, 550$ and 770 nm
 2 (blue, green and red), the particle number concentration in the submicron N_{fine} (light grey) and
 3 the supermicron N_{coarse} (dark) size ranges and the scattering Angstrom exponent \mathring{A} calculated
 4 between 450 and 770 nm (dark grey). N_{coarse} is plotted using the upper horizontal axis. The top
 5 of the boundary layer Z_b and the wind shear level Z_s are indicated in line and in dashed line
 6 respectively. The height of Z_b was situated below the minimum flight level in F30 and F42.
 7 The height of Z_s was situated below the minimum flight level in F42. Data were corrected for
 8 Standard Temperature and Pressure (STP) using $T = 20^\circ\text{C}$ and $P = 1013.25$ hPa.



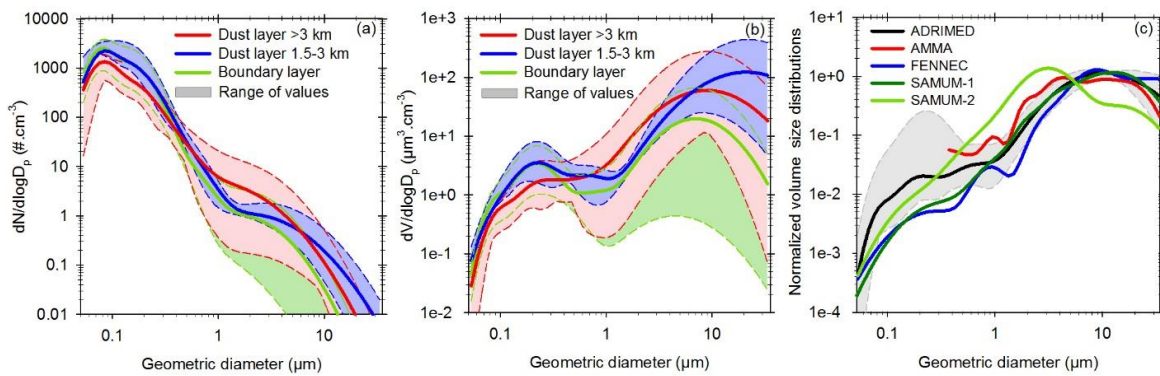
9
 10
 11
 12

1 Figure 6. Five-day backward trajectories calculated for (a) flights F32 and F38 and (b) flight
2 F35 arriving at 2 km asl. and 4 km asl. altitudes in blue and red, respectively.
3



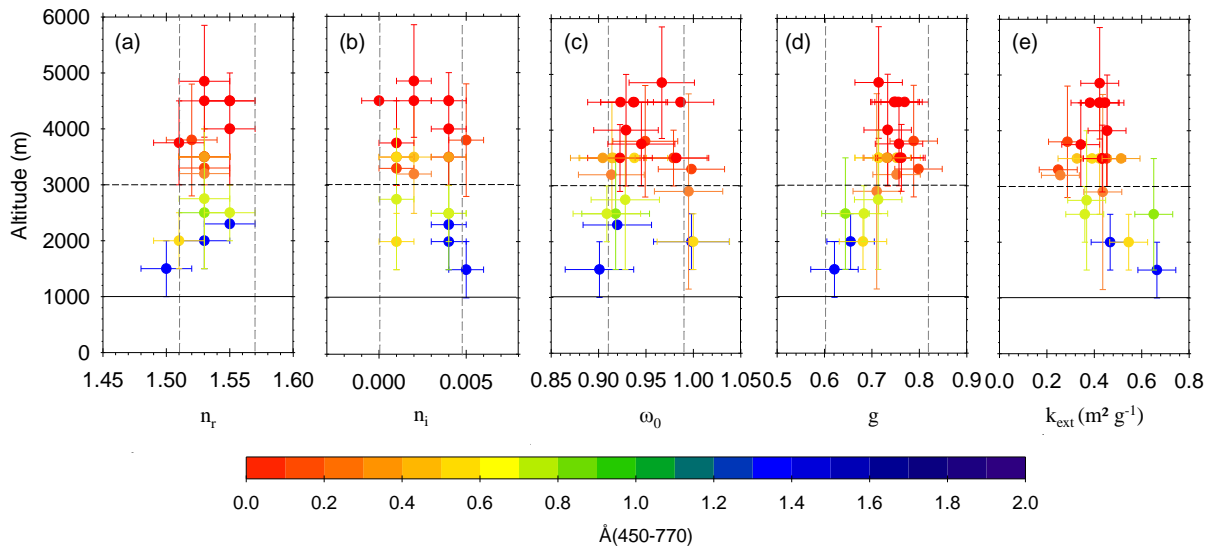
4

1 Figure 7. Particle size distributions obtained in the dust layers during ADRIMED for (a) number
 2 distribution, (b) volume distribution and (c) volume distribution normalized by the total volume
 3 concentration. In Figures (a) and (b), size distributions are classified as a function of the altitude
 4 of the layer: dust layer above 3 km asl (red), dust layer between 1.5-3 km asl (blue) and the
 5 boundary layer below 1 km (green). The shading represents the minimum and maximum
 6 throughout the campaign. In Figure (c), the mean (dark line), minimum and maximum
 7 normalized size distributions (grey shading) observed above 1.5 km during the ADRIMED
 8 campaign are compared with those observed in the source region during the airborne campaigns
 9 AMMA (red line, Formenti et al., 2011a), FENNEC (blue line, Ryder et al., 2013b) and
 10 SAMUM1 (dark green line, Weinzierl et al., 2009), as well as with measurements at Cape-
 11 Verde region during SAMUM-2 campaign (light green line, Weinzierl et al., 2011). The
 12 AMMA curve (Formenti et al., 2011) is curtailed to 0.3 μm since there was no measurement
 13 below this size during the campaign.



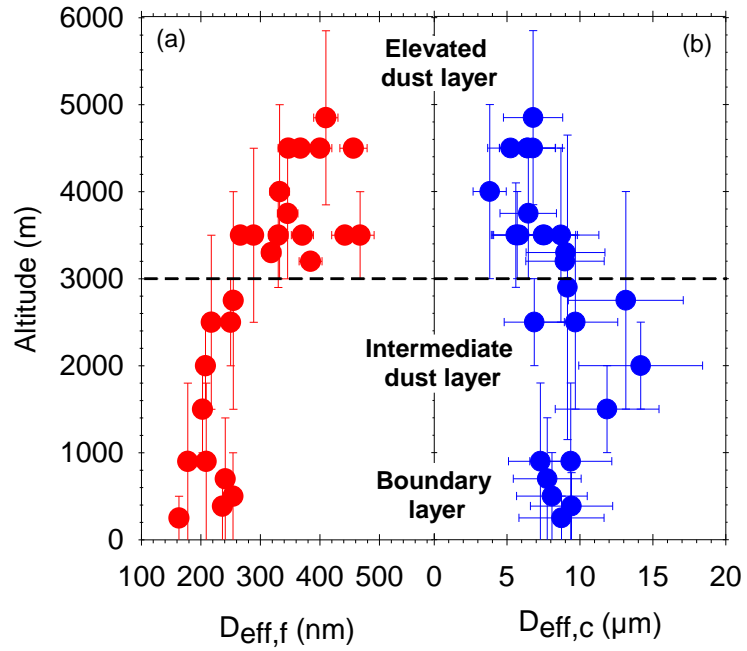
14
 15

1 Figure 8. Scatter plots showing (a) the real part of the complex refractive index, (b) the
 2 imaginary part of the complex refractive index, (c) the single scattering albedo, (d) the
 3 asymmetry parameter and (e) the mass extinction efficiency all at $\lambda=530$ nm as a function of
 4 the altitude from all straight level runs and vertical profiles within the dust layers measured
 5 during the campaign. The altitude indicated for vertical profiles refers to the middle of the layer.
 6 Horizontal error bars display the uncertainties of the parameters. Vertical error bars indicate the
 7 altitude range used to calculate each data point. Broad classifications of the above-3km dust
 8 layer and the below-3km dust layer are shown in horizontal lines. Vertical dashed lines indicate
 9 the range of values obtained in dust source regions. The maximum value of k_{ext} reported in the
 10 literature for dust in source regions is above $0.8 \text{ m}^2 \text{ g}^{-1}$.
 11



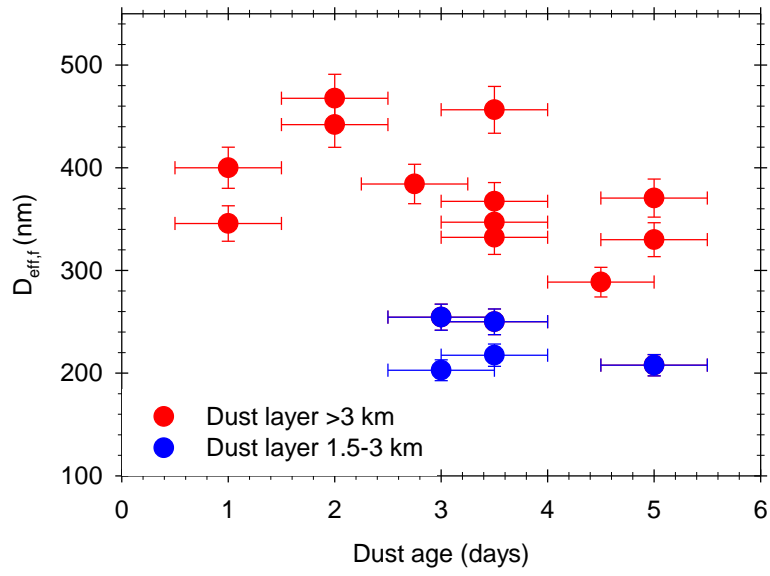
12
 13
 14

1 Figure 9. Altitude dependence of (a) the fine mode effective diameter $D_{eff,f}$ (size range 0.053-1
 2 μm) and (b) the coarse mode effective diameter $D_{eff,c}$ (size range 1-32 μm). The altitude reported
 3 for vertical profiles refers to the middle of the layer. Broad classifications of the above-3km
 4 dust layer, the below-3km dust layer and the boundary layer have been added to the figure.



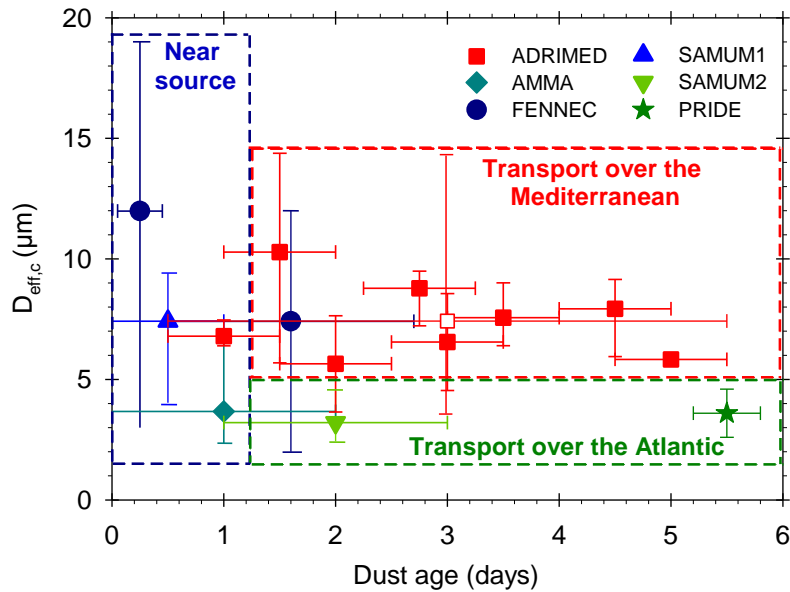
5

1 Figure 10. Effective diameter of the fine mode $D_{eff,f}$ as a function of the dust age observed for
2 the above-3km dust layers (red circles) and the below-3km dust layers (blue circles).
3



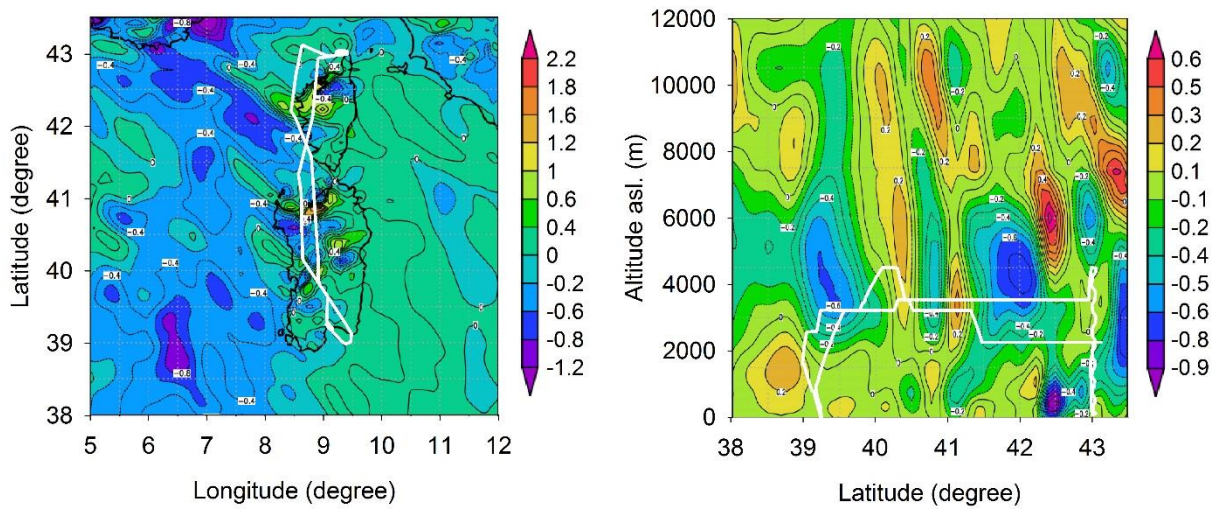
4

1 Figure 11. Effective diameter of the coarse mode $D_{eff,c}$ as a function of the dust age observed
 2 during ADRIMED (squares). Filled red squares represent the average values observed for each
 3 dust age and the empty red square represents the campaign average value. Values are compared
 4 to those observed in dust source region (in blue) during FENNEC (circles), SAMUM1 (triangle)
 5 and AMMA (diamond), as well as measurements in the Atlantic Ocean (in green) at Cape-Verde
 6 region during SAMUM-2 (triangle) and at Puerto-Rico during PRIDE (stars). The horizontal
 7 error bars represent uncertainties on the dust age estimated using HYSPLIT and Seviri RGB
 8 images. The vertical error bars represent the range of values obtained for each dust age.
 9



10

1 Figure 12. 700-hPa vertical velocity field (a) and vertical cross section (b), taken along the F33
2 flight track (white line), from the 10-km resolution WRF model simulations. Values are
3 expressed in Pa s^{-1} .



4

1 References

- 2 Alados-Arboledas, L., Müller, D., Guerrero-Rascado, J. L., Navas-Guzman, D. Pérez-
3 Ramirez, D., and Olmo, F. J. : Optical and microphysical properties of fresh biomass burning
4 aerosol retrieved by Raman lidar, and star-and sun-photometry, *Geophys. Res. Lett.*, 38,
5 L01807, doi:10.1029/2010GL45999.
- 6 Andreae, M. O., and Merlet, P.: Emission of trace gases and aerosols from biomass burning,
7 *Global Biogeochem. Cy.*, 15, 955-966, 10.1029/2000GB001382, 2001.
- 8 Andreae, M. O., and Rosenfeld, D.: Aerosol-cloud-precipitation interactions. Part 1. The
9 nature and sources of cloud-active aerosols, *Earth-Sci. Rev.*, 89, 13-41, 2008.
- 10 Ansmann, A., Baars, H., Tesche, M., Müller, D., Althausen, D., Engelmann, R.,
11 Pauliquevis, T., and Artaxo, P.: Dust and smoke transport from Africa to South America: Lidar
12 profiling over Cape Verde and the Amazon rainforest, *Geophys. Res. Lett.*, 36, L11802,
13 10.1029/2009GL037923, 2009.
- 14 Balkanski, Y., Schulz, M., Claquin, T., and Guibert, S.: Reevaluation of Mineral aerosol
15 radiative forcings suggests a better agreement with satellite and AERONET data, *Atmos. Chem.*
16 *Phys.*, 7, 81-95, doi:10.5194/acp-7-81-2007, 2007
- 17 Basart, S., Pérez, C., Cuevas, E., Baldasano, J. M., and Gobbi, G. P.: Aerosol
18 characterization in Northern Africa, Northeastern Atlantic, Mediterranean Basin and Middle
19 East from direct-sun AERONET observations, *Atmos. Chem. Phys.*, 9, 8265-8282,
20 10.5194/acp-9-8265-2009, 2009.
- 21 Bauer, S.E., Balkanski, Y., Shulz, M., Hauglustaine, D. A., and Dentener F., Global
22 modelling of heterogeneous chemistry on mineral aerosol surfaces: The influence of ozone
23 chemistry and comparison to observations, *L. J. Geophys. Res.*, 109, D02304,
24 doi:10.1029/2003JD003868, 2004.
- 25 Bauer, S. E., Mishchenko, M. I., Lacis, A. A., Zhang, S., Perlwitz, J., and Metzger, S. M.:
26 Do sulphate and nitrate coatings on mineral dust have important effects on radiative properties
27 and climate modeling?, *J. Geophys. Res.-Atmos.*, 112, D06307, 10.1029/2005JD006977, 2007.
- 28 Baumgardner, D., Dye, J. E., Gandrud, B. W., and Knollenberg, R. G.: Interpretation of
29 measurements made by forward scattering probe (FSSP-300) during the airborne arctic
30 stratospheric expedition, *J. Geophys. Res.-Atmos.*, 97, 8035-8046, 1992.
- 31 Baumgardner, D., Popovicheva, O., Allan, J., Bernardoni, V., Cao, J., Cavalli, F., Cozic,
32 J., Diapouli, E., Eleftheriadis, K., Genberg, P. J., Gonzalez, C., Gysel, M., John, A.,
33 Kirchstetter, T. W., Kuhlbusch, T. A. J., Laborde, M., Lack, D., Müller, T., Niessner, R.,
34 Petzold, A., Piazzalunga, A., Putaud, J. P., Schwarz, J., Sheridan, P., Subramanian, R.,
35 Swietlicki, E., Valli, G., Vecchi, R., and Viana, M.: Soot reference materials for instrument
36 calibration and intercomparisons: a workshop summary with recommendations, *Atmos. Meas.*
37 *Tech.*, 5, 1869-1887, 10.5194/amt-5-1869-2012, 2012.
- 38 Bègue, N., Tulet, P., Chaboureaud, J. P., Roberts, G., Gomes, L., and Mallet, M.: Long-range
39 transport of Saharan dust over northwestern Europe during EUCAARI 2008 campaign:
40 Evolution of dust optical properties by scavenging, *J. Geophys. Res.-Atmos.*, 117, D17201,
41 10.1029/2012jd017611, 2012.
- 42 Birmili, W., Heinke, K., Pitz, M., Matschullat, J., Wiedensohler, A., Cyrus, J., Wichmann,
43 H. E., and Peters, A.: Particle number size distributions in urban air before and after
44 volatilisation, *Atmos. Chem. Phys.*, 10, 4643-4660, 10.5194/acp-10-4643-2010, 2010.
- 45 Bohren, C. F., and Huffman, D. R.: Absorption and scattering of light by small particles,
46 Wiley, New York, 1983.
- 47 Bove, M. C., Brotto, P., Cassola, F., Cuccia, E., Massabò, D., Mazzino, A., Piazzalunga,
48 A., and Prati, P.: An integrated PM2.5 source apportionment study: Positive Matrix
49 Factorization vs. the Chemical Transport Model CAMx, *Atmos. Environ.*, 94, 274-286, 2014.

1 Cai, Y., Montague, D. C., Mooiweer-Bryan, W., and Deshler, T.: Performance
2 characteristics of the ultra high sensitivity aerosol spectrometer for particles between 55 and
3 800 nm: Laboratory and field studies, *J. Aerosol Sci.*, 39, 759-769,
4 10.1016/j.jaerosci.2008.04.007, 2008.

5 Cassola, F., Ferrari, F., Mazzino, and Mazzino, A.: Numerical simulations of
6 Mediterranean heavy precipitation events with the WRF model: A verification exercise using
7 different approaches, *Atmos. Res.*, 164-165, 210-225, 10.1016/j.atmosres.2015.05.010, 2015.

8 Charlson, R. J., Schwartz, S. E., Hales, J. M., Cess, R. D., Coakley, J. A., Hansen, J. E.,
9 and Hofmann, D. J.: Climate forcing by anthropogenic aerosols, *Science*, 255, 423-430,
10 10.1126/science.255.5043.423, 1992.

11 Choobari, O. A., Zawar-Reza, P., and Sturman, A.: The global distribution of mineral dust
12 and its impacts on the climate system: A review, *Atmos. Res.*, 138, 152-165,
13 10.1016/j.atmosres.2013.11.007, 2014.

14 Chou, C., Formenti, P., Maille, M., Ausset, P., Helas, G., Harrison, M., and Osborne, S.:
15 Size distribution, shape, and composition of mineral dust aerosols collected during the African
16 Monsoon Multidisciplinary Analysis Special Observation Period 0: Dust and Biomass-Burning
17 Experiment field campaign in Niger, January 2006, *J. Geophys. Res.-Atmos.*, 113, D00C10,
18 10.1029/2008JD009897, 2008.

19 Clarke, A. D., Shinozuka, Y., Kapustin, V. N., Howell, S., Huebert, B., Doherty, S.,
20 Anderson, T., Covert, D., Anderson, J., Hua, X., Moore, K. G., McNaughton, C., Carmichael,
21 G., and Weber, R.: Size distributions and mixtures of dust and black carbon aerosol in Asian
22 outflow: Physiochemistry and optical properties, *J. Geophys. Res.-Atmos.*, 109, D15S09,
23 10.1029/2003JD004378, 2004.

24 Collaud Coen, M., Weingartner, E., Schaub, D., Hueglin, C., Corrigan, C., Henning, S.,
25 Schwikowski, M., and Baltensperger, U.: Saharan dust events at the Jungfraujoch: detection by
26 wavelength dependence of the single scattering albedo and first climatology analysis, *Atmos.*
27 *Chem. Phys.*, 4, 2465-2480, 10.5194/acp-4-2465-2004, 2004.

28 Crumeyrolle, S., Gomes, L., Tulet, P., Matsuki, A., Schwarzenboeck, A., and Crahan, K.:
29 Increase of the aerosol hygroscopicity by cloud processing in a mesoscale convective system:
30 a case study from the AMMA campaign, *Atmos. Chem. Phys.*, 8, 6907-6924, 10.5194/acp-8-
31 6907-2008, 2008.

32 Cuesta, J., Marsham, J. H., Parker, D. J., and Flamant, C.: Dynamical mechanisms
33 controlling the vertical redistribution of dust and the thermodynamic structure of the West
34 Saharan atmospheric boundary layer during summer, *Atmos. Sci. Lett.*, 10, 34-42,
35 10.1002/asl.207, 2009.

36 d'Almeida, G. A.: A Model for Saharan Dust Transport, *Journal of Climate and Applied*
37 *Meteorology*, 25, 903-916, 10.1175/1520-0450(1986)025<0903:AMFSDT>2.0.CO;2, 1986.

38 DeCarlo, P., Slowik, J., Worsnop, D., Davidovits, P., & Jimenez, J.: Particle Morphology
39 and Density Characterization by Combined Mobility and Aerodynamic Diameter
40 Measurements. Part 1: Theory, *Aerosol Sci. Tech.*, 38, 1185-1205, 2004.

41 de Meij, A., and Lelieveld, J.: Evaluating aerosol optical properties observed by ground-
42 based and satellite remote sensing over the Mediterranean and the Middle East in 2006, *Atmos.*
43 *Res.*, 99, 415-433, 10.1016/j.atmosres.2010.11.005, 2011.

44 Di Biagio, C., di Sarra, A., Meloni, D., Monteleone, F., Piacentino, S., and Sferlazzo, D.:
45 Measurements of Mediterranean aerosol radiative forcing and influence of the single scattering
46 albedo, *J. Geophys. Res.-Atmos.*, 114, D06211, 10.1029/2008JD011037, 2009.

47 Di Biagio, C., Doppler, L., Gaimoz, C., Grand, N., Ancellet, G., Raut, J. C., Beekmann,
48 M., Borbon, A., Sartelet, K., Attié, J. L., Ravetta, F., and Formenti, P.: Continental pollution in
49 the Western Mediterranean Basin: vertical profiles of aerosol and trace gases measured over
50 the sea during TRAQA 2012 and SAFMED 2013, *Atmos. Chem. Phys. Discuss.*, 15, 8283-
51 8328, 10.5194/acpd-15-8283-2015, 2015.

1 Di Iorio, T., di Sarra, A., Sferlazzo, D. M., Cacciani, M., Meloni, D., Monteleone, F., Fuà,
2 D., and Fiocco, G.: Seasonal evolution of the tropospheric aerosol vertical profile in the central
3 Mediterranean and role of desert dust, *J. Geophys. Res.-Atmos.*, 114, D02201,
4 10.1029/2008JD010593, 2009.

5 Draxler, R. R., and Rolph, G. D.: HYSPLIT (HYbrid Single-Particle Lagrangian Integrated
6 Trajectory) Model access via NOAA ARL READY Website
7 (<http://ready.arl.noaa.gov/HYSPLIT.php>). , NOAA Air Resources Laboratory, Silver Spring,
8 MD, 2015.

9 Doherty, O. M., Riemer, N., and Hameed, S.: Saharan mineral dust transport into the
10 Caribbean: Observed atmospheric controls and trends, *J. Geophys. Res.-Atmos.*, 113,
11 10.1029/2007jd009171, 2008.

12 Dulac, F., and Chazette, P.: Airborne study of a multi-layer aerosol structure in the eastern
13 Mediterranean observed with the airborne polarized lidar ALEX during a STAAARTE
14 campaign (7 June 1997), *Atmos. Chem. Phys.*, 3, 1817-1831, 10.5194/acp-3-1817-2003, 2003.

15 Engelstaedter, S., Tegen, I., and Washington, R.: North African dust emissions and
16 transport, *Earth-Sci. Rev.*, 79, 73-100, <http://dx.doi.org/10.1016/j.earscirev.2006.06.004>, 2006.

17 Environmental Modeling Center: The GFS Atmospheric Model. NCEP Office Note 442.
18 National Oceanic and Atmospheric Administration, 2003.

19 Fan, X.-B., Okada, K., Niimura, N., Kai, K., Arao, K., Shi, G.-Y., Qin, Y., and Mitsuta, Y.:
20 Mineral particles collected in china and japan during the same Asian dust-storm event, *Atmos.*
21 *Environ.*, 30, 347-351, [http://dx.doi.org/10.1016/1352-2310\(95\)00271-Y](http://dx.doi.org/10.1016/1352-2310(95)00271-Y), 1996.

22 Flamant, C., Chaboureau, J. P., Parker, D. J., Taylor, C. M., Cammas, J. P., Bock, O.,
23 Timouk, F., and Pelon, J.: Airborne observations of the impact of a convective system on the
24 planetary boundary layer thermodynamics and aerosol distribution in the inter-tropical
25 discontinuity region of the West African Monsoon, *Q. J. Roy. Meteor. Soc.*, 133, 1175-1189,
26 10.1002/qj.97, 2007.

27 Formenti, P., Andreae, M. O., Lange, L., Roberts, G., Cafmeyer, J., Rajta, I., Maenhaut,
28 W., Holben, B. N., Artaxo, P., and Lelieveld, J.: Saharan dust in Brazil and Suriname during
29 the Large-Scale Biosphere-Atmosphere Experiment in Amazonia (LBA) - Cooperative LBA
30 Regional Experiment (CLAIRE) in March 1998, *J. Geophys. Res.-Atmos.*, 106, 14919-14934,
31 10.1029/2000JD900827, 2001.

32 Formenti, P., Elbert, W., Maenhaut, W., Haywood, J., and Andreae, M. O.: Chemical
33 composition of mineral dust aerosol during the Saharan Dust Experiment (SHADE) airborne
34 campaign in the Cape Verde region, September 2000, *J. Geophys. Res.-Atmos.*, 108, 8576,
35 10.1029/2002JD002648, 2003.

36 Formenti, P., Rajot, J. L., Desboeufs, K., Caquineau, S., Chevaillier, S., Nava, S.,
37 Gaudichet, A., Journet, E., Triquet, S., Alfaro, S., Chiari, M., Haywood, J., Coe, H., and
38 Highwood, E.: Regional variability of the composition of mineral dust from western Africa:
39 Results from the AMMA SOP0/DABEX and DODO field campaigns, *J. Geophys. Res.-*
40 *Atmos.*, 113, n/a-n/a, 10.1029/2008JD009903, 2008.

41 Formenti, P., Rajot, J. L., Desboeufs, K., Saïd, F., Grand, N., Chevaillier, S., and
42 Schmechtig, C.: Airborne observations of mineral dust over western Africa in the summer
43 Monsoon season: spatial and vertical variability of physico-chemical and optical properties,
44 *Atmos. Chem. Phys.*, 11, 6387-6410, 10.5194/acp-11-6387-2011, 2011a.

45 Formenti, P., Schütz, L., Balkanski, Y., Desboeufs, K., Ebert, M., Kandler, K., Petzold, A.,
46 Scheuvsens, D., Weinbruch, S., and Zhang, D.: Recent progress in understanding physical and
47 chemical properties of African and Asian mineral dust, *Atmos. Chem. Phys.*, 11, 8231-8256,
48 10.5194/acp-11-8231-2011, 2011b.

49 Formenti, P., Caquineau, S., Desboeufs, K., Klaver, A., Chevaillier, S., Journet, E., and
50 Rajot, J. L.: Mapping the physico-chemical properties of mineral dust in western Africa:

1 mineralogical composition, *Atmos. Chem. Phys.*, 14, 10663-10686, 10.5194/acp-14-10663-
2 2014, 2014.

3 Garrett, T. J., Russell, L. M., Ramaswamy, V., Maria, S. F., and Huebert, B. J.:
4 Microphysical and radiative evolution of aerosol plumes over the tropical North Atlantic Ocean,
5 *J. Geophys. Res.-Atmos.*, 108, 4022, 10.1029/2002JD002228, 2003.

6 Gkikas, A., Houssos, E. E., Hatzianastassiou, N., Papadimas, C. D., and Bartzokas, A.:
7 Synoptic conditions favouring the occurrence of aerosol episodes over the broader
8 Mediterranean basin, *Q. J. Roy. Meteor. Soc.*, 138, 932-949, 10.1002/qj.978, 2012.

9 Ginoux, P., J. M. Prospero, T. E. Gill, N. C. Hsu, and M. Zhao (2012), Global-scale
10 attribution of anthropogenic and natural dust sources and their emission rates based on MODIS
11 Deep Blue aerosol products, *Rev. Geophys.*, 50, RG3005, doi:10.1029/2012RG000388, 2012.

12 Gobbi, G. P., Barnada, F., Giorgi, R., and Santacasa, A.: Altitude-resolved properties of a
13 Saharan dust event over the Mediterranean, *Atmos. environ.*, 34, 5119-5127, 2000.

14 Gómez-Amo, J. L., Pinti, V., Di Iorio, T., di Sarra, A., Meloni, D., Becagli, S., Bellantone,
15 V., Cacciani, M., Fuà, D., and Perrone, M. R.: The June 2007 Saharan dust event in the central
16 Mediterranean: Observations and radiative effects in marine, urban, and sub-urban
17 environments, *Atmos. Environ.*, 45, 5385-5393,
18 <http://dx.doi.org/10.1016/j.atmosenv.2011.06.045>, 2011.

19 Goudie, A. S., and Middleton, N. J.: Saharan dust storms: nature and consequences, *Earth-*
20 *Sci. Rev.*, 56, 179-204, [http://dx.doi.org/10.1016/S0012-8252\(01\)00067-8](http://dx.doi.org/10.1016/S0012-8252(01)00067-8), 2001.

21 Guerrero-Rascado, J. L., Ruiz, B., and Alados-Arboledas, L.: Multi-spectral Lidar
22 characterization of the vertical structure of Saharan dust aerosol over southern Spain, *Atmos.*
23 *Environ.*, 42, 2668-2681, <http://dx.doi.org/10.1016/j.atmosenv.2007.12.062>, 2008.

24 Guieu, C., Loÿe-Pilot, M. D., Ridame, C., and Thomas, C.: Chemical characterization of
25 the Saharan dust end-member: Some biogeochemical implications for the western
26 Mediterranean Sea, *J. Geophys. Res.-Atmos.*, 107, ACH 5-1-ACH 5-11,
27 10.1029/2001JD000582, 2002.

28 Hamonou, E., Chazette, P., Balis, D., Dulac, F., Schneider, X., Galani, E., Ancellet, G., and
29 Papayannis, A.: Characterization of the vertical structure of Saharan dust export to the
30 Mediterranean basin, *J. Geophys. Res.-Atmos.*, 104, 22257-22270, 10.1029/1999JD900257,
31 1999.

32 Haywood, J. M., Johnson, B. T., Osborne, S. R., Baran, A. J., Brooks, M., Milton, S. F.,
33 Mulcahy, J., Walters, D., Allan, R. P., Klaver, A., Formenti, P., Brindley, H. E., Christopher,
34 S., and Gupta, P.: Motivation, rationale and key results from the GERBILS Saharan dust
35 measurement campaign, *Q. J. Roy. Meteor. Soc.*, 137, 1106-1116, 10.1002/qj.797, 2011.

36 Heintzenberg, J.: The SAMUM-1 experiment over Southern Morocco: overview and
37 introduction, *Tellus B*, 61, 2-11, 10.1111/j.1600-0889.2008.00403.x, 2009.

38 Hess, M., Koepke, P., and Schult, I.: Optical Properties of Aerosols and Clouds: The
39 Software Package OPAC, *B. Am. Meteorol. Soc.*, 79, 831-844, 10.1175/1520-
40 0477(1998)079<0831:OPOAAC>2.0.CO;2, 1998.

41 Hinds, W. C.: *Aerosol Technology: Properties, Behavior, and Measurement of Airborne*
42 *Particles*, 2nd Edition. Wiley, New York, 1999.

43 Huneus, N., Chevallier, F., and Boucher, O.: Estimating aerosol emissions by assimilating
44 observed aerosol optical depth in a global aerosol model, *Atmos. Chem. Phys.*, 12, 4585-4606,
45 10.5194/acp-12-4585-2012, 2012.

46 IPCC, fifth assessment report - the physical science basis, <http://www.ipcc.ch>, 2013.

47 Jing, S., Jianping, H., Qiang, F., Minnis, P., Jinming, G., and Jianrong, B.: Estimation of
48 Asian dust aerosol effect on cloud radiation forcing using Fu-Liou radiative model and CERES
49 measurements, *Atmos. Chem. Phys.*, 8, 2763-2771, 10.5194/acp-8-2763-2008, 2008.

1 Junkermann, W.: On the distribution of formaldehyde in the western Po-Valley, Italy,
2 during FORMAT 2002/2003, *Atmos. Chem. Phys.*, 9, 9187-9196, 10.5194/acp-9-9187-2009,
3 2009.

4 Kaaden, N., Massling, A., Schladitz, A., Muller, T., Kandler, K., Schutz, L., Weinzierl, B.,
5 Petzold, A., Tesche, M., Leinert, S., Deutscher, C., Ebert, M., Weinbruch, S., and
6 Wiedensohler, A.: State of mixing, shape factor, number size distribution, and hygroscopic
7 growth of the Saharan anthropogenic and mineral dust aerosol at Tinfou, Morocco, *Tellus B*,
8 61, 51-63, 10.1111/j.1600-0889.2008.00388.x, 2009.

9 Kalashnikova, O. V., and Kahn, R. A.: Mineral dust plume evolution over the Atlantic from
10 MISR and MODIS aerosol retrievals, *J. Geophys. Res.-Atmos.*, 113, n/a-n/a,
11 10.1029/2008JD010083, 2008.

12 Kalnay, E., Kanamitsu, M., Kistler, R., Collins, W., Deaven, D., Gandin, L., Iredell, M.,
13 Saha, S., White, G., Woollen, J., Zhu, Y., Leetmaa, A., Reynolds, R., Chelliah, M., Ebisuzaki,
14 W., Higgins, W., Janowiak, J., Mo, K. C., Ropelewski, C., Wang, J., Jenne, R., and Joseph, D.:
15 The NCEP/NCAR 40-Year Reanalysis Project, *B. Am. Meteorol. Soc.*, 77, 437-471,
16 10.1175/1520-0477(1996)077<0437:TNYRP>2.0.CO;2, 1996.

17 Kandler, K., SchÜTz, L., Deutscher, C., Ebert, M., Hofmann, H., JÄCkel, S., Jaenicke, R.,
18 Knippertz, P., Lieke, K., Massling, A., Petzold, A., Schladitz, A., Weinzierl, B., Wiedensohler,
19 A., Zorn, S., and Weinbruch, S.: Size distribution, mass concentration, chemical and
20 mineralogical composition and derived optical parameters of the boundary layer aerosol at
21 Tinfou, Morocco, during SAMUM 2006, *Tellus B*, 61, 32-50, 10.1111/j.1600-
22 0889.2008.00385.x, 2009.

23 Kanitz, T., Engelmann, R., Heinold, B., Baars, H., Skupin, A., and Ansmann, A.: Tracking
24 the Saharan Air Layer with shipborne lidar across the tropical Atlantic, *Geophys. Res. Lett.*, 41,
25 1044-1050, 10.1002/2013GL058780, 2014.

26 Kaufman, Y. J., Tanré, D., Dubovik, D. O., Karnieli, A., and Remer, L. A.: Absorption of
27 sunlight by dust as inferred from satellite and ground-based remote sensing, *Geophys. Res.*
28 *Lett.*, 28, 1479-1482, 2001.

29 Koçak, M., Theodosi, C., Zarmas, P., Séguret, M. J. M., Herut, B., Kallos, G.,
30 Mihalopoulos, N., Kubilay, N., and Nimmo, M.: Influence of mineral dust transport on the
31 chemical composition and physical properties of the Eastern Mediterranean aerosol, *Atmos.*
32 *Environ.*, 57, 266-277, <http://dx.doi.org/10.1016/j.atmosenv.2012.04.006>, 2012.

33 Koehler, K. A., Kreidenweis, S. M., DeMott, P. J., Petters, M. D., Prenni, A. J., and Carrico,
34 C. M.: Hygroscopicity and cloud droplet activation of mineral dust aerosol, *Geophys. Res. Lett.*,
35 36, L08805, 10.1029/2009GL037348, 2009.

36 Korhonen, H., Napari, I., Timmreck, C., Vehkamäki, H., Pirjola, L., Lehtinen, K. E. J.,
37 Lauri, A., and Kulmala, M.: Heterogeneous nucleation as a potential sulphate-coating
38 mechanism of atmospheric mineral dust particles and implications of coated dust on new
39 particle formation, *J. Geophys. Res.-Atmos.*, 108, 4546, 10.1029/2003JD003553, 2003.

40 Koren, I., Joseph, J. H., and Israelevich, P.: Detection of dust plumes and their sources in
41 northeastern Libya, *Can. J. Remote Sens.*, 29, 792-796, 10.5589/m03-036, 2003.

42 Kutuzov, S., Shahgedanova, M., Mikhalevko, V., Ginot, P., Lavrentiev, I., and Kemp, S.:
43 High-resolution provenance of desert dust deposited on Mt. Elbrus, Caucasus in 2009-2012
44 using snow pit and firn core records, *The Cryosphere*, 7, 1481-1498, 10.5194/tc-7-1481-2013,
45 2013.

46 Laborde, M., Mertes, P., Zieger, P., Dommen, J., Baltensperger, U., and Gysel, M.:
47 Sensitivity of the Single Particle Soot Photometer to different black carbon types, *Atmos. Meas.*
48 *Tech.*, 5, 1031-1043, 10.5194/amt-5-1031-2012, 2012.

49 Lack, D. A., and Cappa, C. D.: Impact of brown and clear carbon on light absorption
50 enhancement, single scatter albedo and absorption wavelength dependence of black carbon,
51 *Atmos. Chem. Phys.*, 10, 4207-4220, 10.5194/acp-10-4207-2010, 2010.

1 Levin, Z., Ganor, E., and Gladstein, V.: The Effects of Desert Particles Coated with Sulfate
2 on Rain Formation in the Eastern Mediterranean, *J. Appl. Meteorol.*, 35, 1511-1523,
3 10.1175/1520-0450(1996)035<1511:TEODPC>2.0.CO;2, 1996.

4 Levin, Z., Teller, A., Ganor, E., and Yin, Y.: On the interactions of mineral dust, sea-salt
5 particles, and clouds: A measurement and modeling study from the Mediterranean Israeli Dust
6 Experiment campaign, *J. Geophys. Res.-Atmos.*, 110, n/a-n/a, 10.1029/2005JD005810, 2005.

7 Liu, Y. G., and Daum, P. H.: Relationship of refractive index to mass density and self-
8 consistency of mixing rules for multicomponent mixtures like ambient aerosols, *J. Aerosol Sci.*,
9 39, 974-986, 10.1016/j.jaerosci.2008.06.006, 2008.

10 Liu, D., Allan, J. D., Young, D. E., Coe, H., Beddows, D., Fleming, Z. L., Flynn, M. J.,
11 Gallagher, M. W., Harrison, R. M., Lee, J., Prevot, A. S. H., Taylor, J. W., Yin, J., Williams,
12 P. I., and Zotter, P.: Size distribution, mixing state and source apportionment of black carbon
13 aerosol in London during wintertime, *Atmos. Chem. Phys.*, 14, 10061-10084, 10.5194/acp-14-
14 10061-2014, 2014.

15 Ma, Q. X., Liu, Y. C., Liu, C., and He, H.: Heterogeneous reaction of acetic acid on MgO,
16 alpha-Al₂O₃, and CaCO₃ and the effect on the hygroscopic behaviour of these particles, *Phys.*
17 *Chem. Chem. Phys.*, 14, 8403-8409, 10.1039/c2cp40510e, 2012.

18 Mahowald, N., Albani, S., Kok, J. F., Engelstaeder, S., Scanza, R., Ward, D. S., and
19 Flanner, M. G.: The size distribution of desert dust aerosols and its impact on the Earth system,
20 *Aeolian Research*, 15, 53-71, <http://dx.doi.org/10.1016/j.aeolia.2013.09.002>, 2014.

21 Mallet, M., Van Dingenen, R., Roger, J. C., Despiiau, S., and Cachier, H.: In situ airborne
22 measurements of aerosol optical properties during photochemical pollution events, *J. Geophys.*
23 *Res.-Atmos.*, 110, 10.1029/2004jd005139, 2005.

24 Mallet, M., Dubovik, O., Nabat, P., Dulac, F., Kahn, R., Sciare, J., Paronis, D., and Léon,
25 J. F.: Absorption properties of Mediterranean aerosols obtained from multi-year ground-based
26 remote sensing observations, *Atmos. Chem. Phys.*, 13, 9195-9210, 10.5194/acp-13-9195-2013,
27 2013.

28 Mallet, M., Dulac, F., Formenti, P., Nabat, P., Sciare, J., Roberts, G., Pelon, J., Ancellet,
29 G., Tanré, D., Parol, F., di Sarra, A., Alados, L., Arndt, J., Auriol, F., Blarel, L., Bourrienne,
30 T., Brogniez, G., Chazette, P., Chevaillier, S., Claeys, M., D'Anna, B., Denjean, C., Derimian,
31 Y., Desboeufs, K., Di Iorio, T., Doussin, J. F., Durand, P., Féron, A., Freney, E., Gaimoz, C.,
32 Goloub, P., Gómez-Amo, J. L., Granados-Muñoz, M. J., Grand, N., Hamonou, E., Jankowiak,
33 I., Jeannot, M., Léon, J. F., Maillé, M., Mailler, S., Meloni, D., Menut, L., Momboisse, G.,
34 Nicolas, J., Podvin, J., Pont, V., Rea, G., Renard, J. B., Roblou, L., Schepanski, K.,
35 Schwarzenboeck, A., Sellegri, K., Sicard, M., Solmon, F., Somot, S., Torres, B., Totems, J.,
36 Triquet, S., Verdier, N., Verwaerde, C., Wenger, J., and Zapf, P.: Overview of the Chemistry-
37 Aerosol Mediterranean Experiment/Aerosol Direct Radiative Forcing on the Mediterranean
38 Climate (ChArMEx/ADRMED) summer 2013 campaign, *Atmos. Chem. Phys. Discuss.*, 15,
39 19615-19727, 10.5194/acpd-15-19615-2015, 2015.

40 Mantas, E., Remoundaki, E., Halari, I., Kassomenos, P., Theodosi, C., Hatzikioseyan, A.,
41 and Mihalopoulos, N.: Mass closure and source apportionment of PM_{2.5} by Positive Matrix
42 Factorization analysis in urban Mediterranean environment, *Atmos. Environ.*, 94, 154-163,
43 <http://dx.doi.org/10.1016/j.atmosenv.2014.05.002>, 2014.

44 Marconi, M., Sferlazzo, D. M., Becagli, S., Bommarito, C., Calzolari, G., Chiari, M., di
45 Sarra, A., Ghedini, C., Gómez-Amo, J. L., Lucarelli, F., Meloni, D., Monteleone, F., Nava, S.,
46 Pace, G., Piacentino, S., Rugi, F., Severi, M., Traversi, R., and Udisti, R.: Saharan dust aerosol
47 over the central Mediterranean Sea: PM₁₀ chemical composition and concentration versus
48 optical columnar measurements, *Atmos. Chem. Phys.*, 14, 2039-2054, 10.5194/acp-14-2039-
49 2014, 2014.

1 Maring, H., Savoie, D. L., Izaguirre, M. A., Custals, L., and Reid, J. S.: Mineral dust aerosol
2 size distribution change during atmospheric transport, *J. Geophys. Res.-Atmos.*, 108,
3 10.1029/2002jd002536, 2003.

4 Massoli, P., Kebejian, P. L., Onasch, T. B., Hills, F. B., and Freedman, A., Aerosol light
5 extinction measurements by Cavity Attenuated Phase Shift (CAPS) Spectroscopy: Laboratory
6 validation and field deployment of a compact aerosol particle extinction monitor, *Aerosol Sci.*
7 *Tech.*, 44:6, 428-435, DOI:10.1080/02786821003716599, 2010.

8 McConnell, C. L., Highwood, E. J., Coe, H., Formenti, P., Anderson, B., Osborne, S., Nava,
9 S., Desboeufs, K., Chen, G., and Harrison, M. A. J.: Seasonal variations of the physical and
10 optical characteristics of Saharan dust: Results from the Dust Outflow and Deposition to the
11 Ocean (DODO) experiment, *J. Geophys. Res.-Atmos.*, 113, 10.1029/2007jd009606, 2008.

12 Meloni, D., di Sarra, A., DeLuisi, J., Di Iorio, T., Fiocco, G., Junkermann, W., and Pace,
13 G.: Tropospheric aerosols in the Mediterranean: 2. Radiative effects through model simulations
14 and measurements, *J. Geophys. Res.-Atmos.*, 108, n/a-n/a, 10.1029/2002JD002807, 2003.

15 Meloni, D., di Sarra, A., Pace, G., and Monteleone, F.: Aerosol optical properties at
16 Lampedusa (Central Mediterranean). 2. Determination of single scattering albedo at two
17 wavelengths for different aerosol types, *Atmos. Chem. Phys.*, 6, 715-727, 10.5194/acp-6-715-
18 2006, 2006.

19 Mentaschi, L., Besio, G., Cassola, F., and Mazzino, A.: Performance evaluation of
20 WavewatchIII in the Mediterranean Sea, *Ocean Model.*, 90, 82-94,
21 10.1016/j.ocemod.2015.04.003, 2015.

22 Mian Chin, Diehl, T., Dubovick, O., Eck, T. F., Holben, B. N., Sinyiuk, A., and Streets, D.
23 G.: Light absorption by pollution, dust, and biomass burning aerosols: a global model study and
24 evaluation with AERONET measurements, *Ann. Geophys.*, 27, 3439-3464, doi:10.5194/angeo-
25 27-3439-2009, 2009.

26 Mishchenko, M. I., Lacis, A. A., Carlson, B. E., and Travis, L. D. : Nonsphericity of dust-
27 like tropospheric aerosols : implications for aerosol remote sensing and climate modelling,
28 *Geophys. Res. Lett.*, 22(9), 1077-1080, 1995.

29 Mona, L., Amodeo, A., Pandolfi, M., and Pappalardo, G.: Saharan dust intrusions in the
30 Mediterranean area: Three years of Raman lidar measurements, *J. Geophys. Res.-Atmos.*, 111,
31 D16203, 10.1029/2005JD006569, 2006.

32 Moteki, N., and Kondo, Y.: Dependence of Laser-Induced Incandescence on Physical
33 Properties of Black Carbon Aerosols: Measurements and Theoretical Interpretation, *Aerosol*
34 *Sci.Tech.*, 44, 663-675, 10.1080/02786826.2010.484450, 2010.

35 Moulin, C., Lambert, C. E., Dulac, F., and Dayan, U.: Control of atmospheric export of
36 dust from North Africa by the North Atlantic Oscillation, *Nature*, 387, 691-694, 1997.

37 Moulin, C., Lambert, C. E., Dayan, U., Masson, V., Ramonet, M., Bousquet, P., Legrand,
38 M., Balkanski, Y. J., Guelle, W., Marticorena, B., Bergametti, G., and Dulac, F.: Satellite
39 climatology of African dust transport in the Mediterranean atmosphere, *J. Geophys. Res.-*
40 *Atmos.*, 103, 13137-13144, 10.1029/98JD00171, 1998.

41 Moulin, C., Gordon, H. R., Banzon, V. F., and Evans, R. H.: Assessment of Saharan dust
42 absorption in the visible from Sea- WiFS imagery, *J. Geophys. Res.*, 106(D16), 18 239–18 250,
43 doi:10.1029/2000JD900812, 2001.

44 Muller, T., Laborde, M., Kassell, G., and Wiedensohler, A.: Design and performance of a
45 three-wavelength LED-based total scatter and backscatter integrating nephelometer, *Atmos.*
46 *Meas. Tech.*, 4., 1291-1303, doi:10.5194/amt-4-1291-2011, 2011a.

47 Muller, T., Schladitz, A., Kandler, K., and Wiedensohler, A.: Spectral particle absorption
48 coefficients, single scattering albedos and imaginary parts of refractive indices from ground
49 based in situ measurements at Cape Verde Island during SAMUM-2, *Tellus B*, 63, 573-588,
50 10.1111/j.1600-0889.2011.00572.x, 2011b.

1 Nabat, P., Solmon, F., Mallet, M., Michou, M., Sevault, F., Driouech, F., Meloni, D., di
2 Sarra, A., Di Biagio, C., Formenti, P., Sicard, M., Léon, J.-F., and Bouin, M. -N.: Dust aerosol
3 radiative effects during summer 2012 simulated with a coupled regional aerosol-atmosphere-
4 ocean model over the Mediterranean, *Atmos. Chem. Phys.*, 15, 3303-3326, doi:10.5194/acp-
5 15-3303-2015, 2015.

6 Osborne, S. R., Johnson, B. T., Haywood, J. M., Baran, A. J., Harrison, M. A. J., and
7 McConnell, C. L.: Physical and optical properties of mineral dust aerosol during the Dust and
8 Biomass-burning Experiment, *J. Geophys. Res.-Atmos.*, 113, 10.1029/2007jd009551, 2008.

9 Otto, S., Bierwirth, E., Weinzierl, B., Kandler, K., Esselborn, M., Tesche, M., Schladitz,
10 A., Wendisch, M., and Trautmann, T.: Solar radiative effects of a Saharan dust plume observed
11 during SAMUM assuming spheroidal model particles, *Tellus B*, 61, 270-296, 10.1111/j.1600-
12 0889.2008.00389.x, 2009.

13 Pace, G., Meloni, D., and di Sarra, A.: Forest fire aerosol over the Mediterranean basin
14 during summer 2003, *J. Geophys. Res.*, 110, D21202, doi:10.1029/2005JD005986, 2005.

15 Papayannis, A., Amiridis, V., Mona, L., Tsaknakis, G., Balis, D., Bosenberg, J.,
16 Chaikovski, A., De Tomasi, F., Grigorov, I., Mattis, I., Mitev, V., Muller, D., Nickovic, S.,
17 Perez, C., Pietruczuk, A., Pisani, G., Ravetta, F., Rizi, V., Sicard, M., Trickl, T., Wiegner, M.,
18 Gerding, M., Mamouri, R. E., D'Amico, G., and Pappalardo, G.: Systematic lidar observations
19 of Saharan dust over Europe in the frame of EARLINET (2000-2002), *J. Geophys. Res.-
20 Atmos.*, 113, 10.1029/2007jd009028, 2008.

21 Perrone, M. R., and Bergamo, A.: Direct radiative forcing during Sahara dust intrusions at
22 a site in the Central Mediterranean: Anthropogenic particle contribution, *Atmos. Res.*, 101, 783-
23 798, 10.1016/j.atmosres.2011.05.011, 2011.

24 Perry, K. D., Cahill, T. A., Eldred, R. A., Dutcher, D. D., and Gill, T. E.: Long-range
25 transport of North African dust to the eastern United States, *J. Geophys. Res.-Atmos.*, 102,
26 11225-11238, 10.1029/97JD00260, 1997.

27 Petzold, A., Rasp, K., Weinzierl, B., Esselborn, M., Hamburger, T., DÖRnbrack, A.,
28 Kandler, K., SchÜTz, L., Knippertz, P., Fiebig, M., and Virkkula, A. K. I.: Saharan dust
29 absorption and refractive index from aircraft-based observations during SAMUM 2006, *Tellus
30 B*, 61, 118-130, 10.1111/j.1600-0889.2008.00383.x, 2009.

31 Pey, J., Querol, X., Alastuey, A., Forastiere, F., and Stafoggia, M.: African dust outbreaks
32 over the Mediterranean Basin during 2001–2011: PM10 concentrations,
33 phenomenology and trends, and its relation with synoptic and mesoscale meteorology, *Atmos.
34 Chem. Phys.*, 13, 1395-1410, 10.5194/acp-13-1395-2013, 2013.

35 Prospero, J. M., Ginoux, P., Torres, O., Nicholson, S. E., and Gill, T. E.: Environmental
36 characterization of global sources of atmospheric soil dust identified with the nimbus 7 total
37 ozone mapping spectrometer (TOMS) absorbing aerosol product, *Rev. Geophys.*, 40, 1002,
38 10.1029/2000RG000095, 2002.

39 Querol, X., Alastuey, A., Pey, J., Cusack, M., Pérez, N., Mihalopoulos, N., Theodosi, C.,
40 Gerasopoulos, E., Kubilay, N., and Koçak, M.: Variability in regional background aerosols
41 within the Mediterranean, *Atmos. Chem. Phys.*, 9, 4575-4591, 10.5194/acp-9-4575-2009, 2009.

42 Reid, J. S., Kinney, J. E., Westphal, D. L., Holben, B. N., Welton, E. J., Tsay, S.-C.,
43 Eleuterio, D. P., Campbell, J. R., Christopher, S. A., Colarco, P. R., Jonsson, H. H., Livingston,
44 J. M., Maring, H. B., Meier, M. L., Pilewskie, P., Prospero, J. M., Reid, E. A., Remer, L. A.,
45 Russell, P. B., Savoie, D. L., Smirnov, A., and Tanré, D.: Analysis of measurements of Saharan
46 dust by airborne and ground-based remote sensing methods during the Puerto Rico Dust
47 Experiment (PRIDE), *J. Geophys. Res.-Atmos.*, 108, 8586, 10.1029/2002JD002493, 2003.

48 Ripoll, A., Minguillón, M. C., Pey, J., Pérez, N., Querol, X., and Alastuey, A.: Joint analysis
49 of continental and regional background environments in the western Mediterranean: PM1 and
50 PM10 concentrations and composition, *Atmos. Chem. Phys.*, 15, 1129-1145, 10.5194/acp-15-
51 1129-2015, 2015.

1 Rosenberg, P. D., Parker, D. J., Ryder, C. L., Marsham, J. H., Garcia-Carreras, L., Dorsey,
2 J. R., Brooks, I. M., Dean, A. R., Crosier, J., McQuaid, J. B., and Washington, R.: Quantifying
3 particle size and turbulent scale dependence of dust flux in the Sahara using aircraft
4 measurements, *J. Geophys. Res.-Atmos.*, 119, 7577-7598, 10.1002/2013JD021255, 2014.

5 Rosenfeld, D., Rudich, Y., and Lahav, R.: Desert dust suppressing precipitation: A possible
6 desertification feedback loop, *P. Natl. Ac. Sci.*, 98, 5975-5980, 10.1073/pnas.101122798, 2001.

7 Ryder, C. L., Highwood, E. J., Lai, T. M., Sodemann, H., and Marsham, J. H.: Impact of
8 atmospheric transport on the evolution of microphysical and optical properties of Saharan dust,
9 *Geophys. Res. Lett.*, 40, 2433-2438, 10.1002/grl.50482, 2013a.

10 Ryder, C. L., Highwood, E. J., Rosenberg, P. D., Trembath, J., Brooke, J. K., Bart, M.,
11 Dean, A., Crosier, J., Dorsey, J., Brindley, H., Banks, J., Marsham, J. H., McQuaid, J. B.,
12 Sodemann, H., and Washington, R.: Optical properties of Saharan dust aerosol and contribution
13 from the coarse mode as measured during the Fennec 2011 aircraft campaign, *Atmos. Chem.*
14 *Phys.*, 13, 303-325, 10.5194/acp-13-303-2013, 2013b.

15 Saha, A., Mallet, M., Roger, J. C., Dubuisson, P., Piazzola, J., and Despiiau, S.: One year
16 measurements of aerosol optical properties over an urban coastal site: Effect on local direct
17 radiative forcing, *Atmos. Res.*, 90, 195-202, <http://dx.doi.org/10.1016/j.atmosres.2008.02.003>,
18 2008.

19 Saha, S., Moorthi, S., Pan, H.-L., Wu, X., Wang, J., Nadiga, S., Tripp, P., Kistler, R.,
20 Woollen, J., Behringer, D., Liu, H., Stokes, D., Grumbine, R., Gayno, G., Wang, J., Hou, Y.-
21 T., Chuang, H.-Y., Juang, H.-M. H., Sela, J., Iredell, M., Treadon, R., Kleist, D., Van Delst, P.,
22 Keyser, D., Derber, J., Ek, M., Meng, J., Wei, H., Yang, R., Lord, S., Van Den Dool, H., Kumar,
23 A., Wang, W., Long, C., Chelliah, M., Xue, Y., Huang, B., Schemm, J.-K., Ebisuzaki, W., Lin,
24 R., Xie, P., Chen, M., Zhou, S., Higgins, W., Zou, C.-Z., Liu, Q., Chen, Y., Han, Y., Cucurull,
25 L., Reynolds, R. W., Rutledge, G., and Goldberg, M.: The NCEP Climate Forecast System
26 Reanalysis, *B. Am. Meteorol. Soc.*, 91, 1015-1057, 10.1175/2010BAMS3001.1, 2010.

27 Saïd, F., Canut, G., Durand, P., Lohou, F., and Lothon, M.: Seasonal evolution of boundary-
28 layer turbulence measured by aircraft during the AMMA 2006 Special Observation Period, *Q.*
29 *J. Roy. Meteor. Soc.*, 136, 47-65, 10.1002/qj.475, 2010.

30 Salvador, P., Alonso-Pérez, S., Pey, J., Artíñano, B., de Bustos, J. J., Alastuey, A., and
31 Querol, X.: African dust outbreaks over the western Mediterranean Basin: 11-year
32 characterization of atmospheric circulation patterns and dust source areas, *Atmos. Chem. Phys.*,
33 14, 6759-6775, 10.5194/acp-14-6759-2014, 2014.

34 Scheuvens, D., Schütz, L., Kandler, K., Ebert, M., and Weinbruch, S.: Bulk composition of
35 northern African dust and its source sediments — A compilation, *Earth-Sci. Rev.*, 116, 170-
36 194, <http://dx.doi.org/10.1016/j.earscirev.2012.08.005>, 2013.

37 Schladitz, A., Müller, T., Kaaden, N., Massling, A., Kandler, K., Ebert, M., Weinbruch, S.,
38 Deutscher, C., and Wiedensohler, A.: In situ measurements of optical properties at Tinfou
39 (Morocco) during the Saharan Mineral Dust Experiment SAMUM 2006, *Tellus B*, 61, 64-78,
40 10.1111/j.1600-0889.2008.00397.x, 2009.

41 Schladitz, A., MÜLLER, T., Nordmann, S., Tesche, M., Groß, S., Freudenthaler, V.,
42 Gasteiger, J., and Wiedensohler, A.: In situ aerosol characterization at Cape Verde, *Tellus B*,
43 63, 549-572, 10.1111/j.1600-0889.2011.00568.x, 2011.

44 Seinfeld, J. H., and Pandis, S. N.: *Atmospheric chemistry and physics: From air pollution*
45 *to climate change*, 714 pp., 1998.

46 Sicard, M., Mallet, M., García-Vizcaíno, D., Comerón, A., Rocadenbosch, F., Dubuisson,
47 P., and Muñoz-Porcar, C.: Intense dust and extremely fresh biomass burning outbreak in
48 Barcelona, Spain: characterization of their optical properties and estimation of their direct
49 radiative forcing, *Environ. Res. Lett.*, 7, 034016, 2012.

50 Sicard, M., Bertolín, S., Mallet, M., Dubuisson, P., and Comerón, A.: Estimation of mineral
51 dust long-wave radiative forcing: sensitivity study to particle properties and application to real

1 cases in the region of Barcelona, *Atmos. Chem. Phys.*, 14, 9213-9231, 10.5194/acp-14-9213-
2 2014, 2014.

3 Skamarock, W. C., Klemp, J. B., Dudhia, J., Gill, D. O., Barker, D. M., Huang, X. Z.,
4 Wang, W., and Powers, J. G.: A Description of the Advanced Research WRF Version 3.
5 Technical report. Mesoscale and Microscale Meteorology Division, NCAR, Boulder, Colorado,
6 2008.

7 Sokolik, I. N., and Toon, O. B.: Direct radiative forcing by anthropogenic airborne mineral
8 aerosols, *Nature*, 381, 681-683, 1996.

9 Sullivan, A. P., and Weber, R. J.: Chemical characterization of the ambient organic aerosol
10 soluble in water: 2. Isolation of acid, neutral, and basic fractions by modified size-exclusion
11 chromatography, *J. Geophys. Res.*, 111, D05315, 2006.

12 Sullivan, R. C., and Prather, K. A.: Investigations of the Diurnal Cycle and Mixing State of
13 Oxalic Acid in Individual Particles in Asian Aerosol Outflow, *Environ. Sci. Technol.*, 41, 8062-
14 8069, 10.1021/es071134g, 2007.

15 Sullivan, R. C., Moore, M. J. K., Petters, M. D., Kreidenweis, S. M., Roberts, G. C., and
16 Prather, K. A.: Effect of chemical mixing state on the hygroscopicity and cloud nucleation
17 properties of calcium mineral dust particles, *Atmos. Chem. Phys.*, 9, 3303-3316, 2009.

18 Swap, R., Garstang, M., Greco, S., Talbot, R., and KÅLLberg, P.: Saharan dust in the
19 Amazon Basin, *Tellus B*, 44, 133-149, 10.1034/j.1600-0889.1992.t01-1-00005.x, 1992.

20 Tegen, I., and Lacis, A. A.: Modeling of particle size distribution and its influence on the
21 radiative properties of mineral dust aerosol, *J. Geophys. Res.-Atmos.*, 101, 19237-19244,
22 10.1029/95JD03610, 1996.

23 Trochline, D., Iwasaka, Y., Matsuki, A., Yamada, M., Kim, Y. S., Nagatani, T., Zhang, D.,
24 Shi, G. Y., and Shen, Z.: Mineral aerosol particles collected in Dunhuang, China, and their
25 comparison with chemically modified particles collected over Japan, *J. Geophys. Res.-Atmos.*,
26 108, 8642, 10.1029/2002JD003268, 2003.

27 Tsyro, S., Simpson, D., Tarrasón, L., Klimont, Z., Kupiainen, K., Pio, C., and Yttri, K. E.:
28 Modeling of elemental carbon over Europe, *J. Geophys. Res.-Atmos.*, 112, D23S19,
29 10.1029/2006JD008164, 2007.

30 Ullerstam, M., Vogt, R., Langer, S., and Ljungstrom, E.: The kinetics and mechanism of
31 SO₂ oxidation by O₃ on mineral dust, *Phys. Chem. Chem. Phys.*, 4, 4694-4699,
32 10.1039/B203529B, 2002.

33 Valenzuela, A., Olmo, F. J., Lyamani, H., Granados-Muñoz, M. J., Antón, M., Guerrero-
34 Rascado, J. L., Quirantes, A., Toledano, C., Perez-Ramírez, D., and Alados-Arboledas, L.:
35 Aerosol transport over the Western Mediterranean basin: Evidence of fine particles to desert
36 plumes over Alboran Island, *J. Geophys. Res.-Atmos.*, 2014JD022044,
37 10.1002/2014JD022044, 2014.

38 Van Dingenen, R., Putaud, J.-P., Martins-Dos Santos, S., and Raes, F.: Physical aerosol
39 properties and their relation to air mass origin at Monte Cimone (Italy) during the first
40 MINATROC campaign, *Atmos. Chem. Phys.*, 5, 2203-2226, doi:10.5194/acp-5-2203-2005,
41 2005.

42 Villani, P., Picard, D., Marchand, N., and Laj, P.: Design and Validation of a 6-Volatility
43 Tandem Differential Mobility Analyzer (VTDMA), *Aerosol Sci. Tech.*, 41, 898-906,
44 10.1080/02786820701534593, 2007.

45 Weinzierl, B., Petzold, A., Esselborn, M., Wirth, M., Rasp, K., Kandler, K., SchÜTZ, L.,
46 Koepke, P., and Fiebig, M.: Airborne measurements of dust layer properties, particle size
47 distribution and mixing state of Saharan dust during SAMUM 2006, *Tellus B*, 61, 96-117,
48 10.1111/j.1600-0889.2008.00392.x, 2009.

49 Weinzierl, B., Sauer, D., Esselborn, M., Petzold, A., Veira, A., Rose, M., Mund, S., Wirth,
50 M., Ansmann, A., Tesche, M., Gross, S., and Freudenthaler, V.: Microphysical and optical
51 properties of dust and tropical biomass burning aerosol layers in the Cape Verde region-an

1 overview of the airborne in situ and lidar measurements during SAMUM-2, *Tellus B*, 63, 589-
2 618, 10.1111/j.1600-0889.2011.00566.x, 2011.

3 Wiedensohler, A., Birmili, W., Nowak, A., Sonntag, A., Weinhold, K., Merkel, M.,
4 Wehner, B., Tuch, T., Pfeifer, S., Fiebig, M., Fjåraa, A. M., Asmi, E., Sellegri, K., Depuy, R.,
5 Venzac, H., Villani, P., Laj, P., Aalto, P., Ogren, J. A., Swietlicki, E., Williams, P., Roldin, P.,
6 Quincey, P., Hüglin, C., Fierz-Schmidhauser, R., Gysel, M., Weingartner, E., Riccobono, F.,
7 Santos, S., Gruning, C., Faloon, K., Beddows, D., Harrison, R., Monahan, C., Jennings, S. G.,
8 O'Dowd, C. D., Marinoni, A., Horn, H. G., Keck, L., Jiang, J., Scheckman, J., McMurry, P. H.,
9 Deng, Z., Zhao, C. S., Moerman, M., Henzing, B., de Leeuw, G., Löschau, G., and Bastian, S.:
10 Mobility particle size spectrometers: harmonization of technical standards and data structure to
11 facilitate high quality long-term observations of atmospheric particle number size distributions,
12 *Atmos. Meas. Tech.*, 5, 657-685, 10.5194/amt-5-657-2012, 2012.

13 Zhou, M., Okada, K., Qian, F., Wu, P. M., Su, L., Casareto, B. E., and Shimohara, T.:
14 Characteristics of dust-storm particles and their long-range transport from China to Japan - case
15 studies in April 1993, *Atmos. Res.*, 40, 19-31, [http://dx.doi.org/10.1016/0169-8095\(95\)00023-](http://dx.doi.org/10.1016/0169-8095(95)00023-2)
16 2, 1996.

17